Graphical Abstract

Click here to download Graphical Abstract Graphical Abstract.pdf

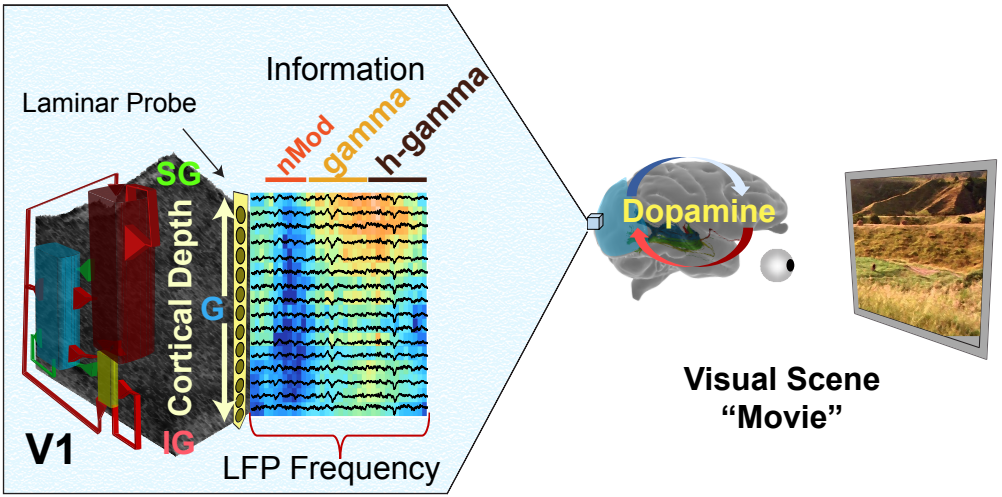

Dopamine is signaled by mid-frequency oscillations and boosts output-layers visual information in visual cortex

Daniel Zaldivar[1,2,*], Jozien Goense[3,≠], Scott C. Lowe[4], Nikos K. Logothetis[1,5], Stefano Panzeri[6,*,≠]

[1] Max Planck Institute for Biological Cybernetics; Spemannstrasse 38, D-72076 Tübingen, Germany.
[2] IMPRS for Cognitive and Systems Neuroscience, University of Tübingen; Österbergstrasse 3, D-72074 Tübingen, Germany
[3] School of Psychology and Institute of Neuroscience and Psychology, University of Glasgow; 58 Hillhead Street, Glasgow G12 8QB, United Kingdom
[4] Institute for Adaptive and Neural Computation, School of Informatics, University of Edinburgh, EH8 9AB, United Kingdom
[5] Division of Imaging Science and Biomedical Engineering, University of Manchester; Manchester M13 9PT, United Kingdom
[6] Center for Neuroscience and Cognitive Systems, Istituto Italiano di Tecnologia, 38068 Rovereto, Italy.

* Corresponding Authors
Daniel Zaldivar; Daniel.Zaldivar@tuebingen.mpg.de
Stefano Panzeri; Stefano.Panzeri@iit.it

≠ Co-senior author

Lead Contact: Daniel Zaldivar (Daniel.zaldivar@tuebingen.mpg.de)

RUNNING TITLE

Dopamine and oscillatory information processing in macaque V1

SUMMARY

Neural oscillations are ubiquitously observed in cortical activity, and are widely believed to be crucial for mediating transmission of information across the cortex. Yet, the neural phenomena contributing to each oscillation band, and their effect on information coding and transmission, are largely unknown. Here, we investigated if individual frequency bands specifically reflect changes in the concentrations of dopamine, an important neuromodulator, and how dopamine affects oscillatory information processing. We recorded the LFP at different depths of V1 in anesthetized monkeys (*macaca mulatta*) during spontaneous activity and during visual stimulation with Hollywood movie clips, while pharmacologically mimicking dopaminergic neuromodulation by systemic injection of L-DOPA (a metabolic precursor of dopamine). We found that dopaminergic neuromodulation had marked effects on both spontaneous and movie-evoked neural activity. During spontaneous activity, dopaminergic neuromodulation increased the power of the LFP specifically in the [19–38 Hz] band, suggesting that the power of endogenous visual cortex oscillations in this band can be used as a robust marker of dopaminergic neuromodulation. Moreover, dopamine increased visual information encoding over all frequencies during movie stimulation. The information increase due to dopamine was prominent in the supragranular layers of cortex that project to higher cortical areas and in the gamma [50–100 Hz] band that has been previously implicated in mediating feedforward information transfer. These results thus individuate new neural mechanisms by which dopamine may promote the readout of relevant sensory information by strengthening the transmission of information from primary to higher areas.

Key words: Primary visual cortex (V1); local field potentials (LFPs); cortical layers; Information Theory; Dopaminergic neuromodulation.

INTRODUCTION

An animal's response to sensory stimuli depends not only on the stimulus but also on the animal's cognitive state. These cognitive states are influenced by diverse neuromodulators that change brain states and enable circuits of neurons to modulate how they encode and process information, when the behavioral context or the stimulus processing or cognitive demands vary [1, 2]. Documenting the effects of neuromodulators on neural information processing is thus essential to understand the neural bases of adaptive computations. Furthermore, identifying signatures of neuromodulation-induced changes in neural activity is key to revealing the potential causes of cognitive deficits and of pathophysiology of brain disorders [3].

A prominent and robustly observed feature of cortical activity is the presence of oscillations spanning several octaves of frequency [4, 5]. Oscillations have been implicated in several flexible brain computations, including sensory coding [6-9] and dynamical modulation of information transmission along feedforward, lateral and feedback pathways [8, 10, 11]. Moreover, oscillations have been used widely to investigate brain activity during cognitive tasks that likely engage neuromodulation, or in brain pathologies potentially related to neuromodulation dysfunction [2, 12]. Thus, understanding how different frequency bands capture changes in neuromodulators and their effect in dynamically regulating information processing is paramount.

To shed light on these issues, here we experimentally investigated the role of dopamine (DA), a major neuromodulator, in shaping oscillatory visual information processing. We used laminar probes to simultaneously record Local Field Potentials (LFPs), a signal suited to capture mescoscopic oscillatory activity, at different depths of V1. We investigated the effects of systemically injected L-DOPA (a metabolic precursor of DA) in anesthetized monkeys during both spontaneous activity and during presentations of naturalistic movies. We focused on the effects of systemic application of DA on visual cortex, for multiple reasons. First, it has been

shown that systemic injection of L-DOPA benefits early visual processing in Parkinson's disease patients [13] and treats effectively amblyopia [14, 15]. This suggests that, even if V1 lacks DA-receptors [16, 17], systemic injection of DA may modulate early visual cortical function [18], for example through top-down cortico-cortical interactions [18-22]. Second, in our previous studies we individuated in V1 LFPs an oscillatory band, with a frequency [19–38 Hz] slow enough to be possibly mediated by longer-range interactions, that exhibited the statistical signatures of a band driven by neuromodulation [6], and we wished to determine causally its origin by pharmacological intervention.

RESULTS

We simultaneously recorded the local field potential (LFP) from the different laminae of area V1 of anaesthetized macaque monkeys using a laminar, vertically inserted, linear probe with 16 contacts spaced 150 μm apart (Figure 1). We recorded a total of 15 experimental sessions in 4 different animals (STAR Methods). One or two pharmacological injections were acquired each day. After each experiment, monkeys were rested for 15 days.

To determine the cortical depth and layer of each electrode, we used the current source density (CSD) extracted from the laminar LFP (Figure 1C and S2A). The CSD estimates the net current density entering or leaving the extracellular medium [10, 23]. The CSD pattern was used to assign electrode sites to either supragranular- (SG), granular (G) or infragranular (IG) layers. We used each session's trial-averaged CSD (Figure 1C shows the average over sessions), computed after the onset of the movie, to identify the border between G and IG layers (bottom end of the sink at 40–60 ms after movie onset; STAR Methods). The G/IG border was identified [24-27] as the point with a sudden drop in LFP gamma-band coherence (Eq. 1, STAR Methods; Figure 1D, S2B). The cortical boundaries and the location of the SG/G boundary were determined using the average thickness of cortical layers in macaque V1 [28-30].

To investigate both endogenous and stimulus-driven processes, our stimulus protocol consisted of a block paradigm alternating Hollywood movie-clips (20 s) with 20 s isoluminant gray screen periods before and after each clip (Figure 1A, top panel). Such movies contain a wide range of naturalistic variations of visual features (movie temporal spectra are shown in Figure 2C) and thus elicit a rich spectrum of LFP activity likely capturing several distinct neural processes [6, 31, 32]. Using techniques developed in our previous work [18, 33], we mimicked an increase of dopaminergic- (DAergic-) neuromodulation by systemic injection (injection period of 12 min, corresponding to 12 visual stimulation blocks) of L-DOPA and Carbidopa (2.1 mg/kg and 0.5 mg/kg, respectively [34]). This pharmacological approach is widely used for the treatment of Parkinson's disease patients and it has also been shown to be effective in treating amblyopia [14]. L-DOPA metabolizes to DA once it crosses the blood-brain barrier. Carbidopa prevents the breakdown of L-DOPA in the periphery, thereby increasing the amount of L-DOPA crossing the blood-brain barrier. Systemic L-DOPA injections are known to modulate V1 activity, unlike its local application, suggesting that DA modulates V1 indirectly, possibly through cortico-cortical pathways [18].

Visually Driven and Spontaneous Oscillatory Activity in V1 Before Dopamine Injection

As a preliminary step, we identified the LFP frequency bands that are most relevant for visual coding before DA injection, without specificity to the laminar location. These were then selected for further investigation.

Figure 2A shows the LFP power spectrum averaged over all electrode sites in all sessions (Figure S1A-B shows spectra for individual sessions). These spectra were similar to those previous observed under similar anesthesia [6]. Oscillatory activity had significant power ($p=0.0012$; t-test) over the entire frequency range (1–150 Hz) for both spontaneous and stimulus-evoked activity. The power of movie-evoked activity increased over that of spontaneous activity throughout the spectrum (Figure 2A). Consistent with previous studies

[6, 35, 36], the larger movie-evoked power increase occurred in the gamma (γ, 50–100 Hz) and high-γ (101–150 Hz) bands.

To quantify the visual coding capacity of each frequency, we computed the mutual information [37] that the LFP-power, at each frequency, conveys about the section of the movie being presented (STAR methods). This measure, in units of bits, captures the information about all possible visual attributes occurring in the movies and does not depend on assumptions about which features in the movie are encoded by the power [6, 38]. Results, averaged over all electrodes in all sessions, are shown in Figure 2B. In agreement with earlier data recorded in V1 under the same anesthesia but with electrodes that lacked laminar resolution [6, 31], we found two informative bands in the LFP spectrum: a low-LFP-frequency range (up to 15 Hz, covering the delta (δ), theta (θ), and alpha (α) bands), and a broad high-frequency region covering the γ and high-γ range of 50–150 Hz (Figure 2B). Previous work [6] as well as our further analyses (see below) showed that low and high-frequency LFP-bands carry independent information about the movie, and are thus genuinely different bands.

Despite their relatively high power, LFP-frequencies in the mid-frequency range (19–38 Hz) conveyed much less information about the movie (Figure 2B) and were not reliably stimulus-modulated (Figure S3). This result was consistent with previous studies in monkeys [5, 6] and humans [39]. Given that the power of frequencies in this band is high but carries low visual information, and given the strong correlations within this mid-frequency region (see [6] and later Sections), we previously suggested that this band may capture the fluctuations of sources of stimulus-unrelated neuromodulation. We therefore termed this band "neuromodulation band" [nMOD; see 6, 31]. However, until now the hypothesis that this band reflects neuromodulation has not been causally tested. A goal of this study is to pharmacologically test this hypothesis.

Based on the above results, we singled out four bands for further analysis. Three bands cover the stimulus-informative range: α [8–15 Hz], γ [50–100 Hz] and high-γ [101–150 Hz]. One

band covers the stimulus-unrelated middle-frequency range (nMOD [19–38 Hz]). To avoid biasing the results with the specific choice of bands, we complemented the band-specific analysis with analysis of the power of individual Fourier coefficients.

Layer- and Frequency-Specific Power Changes Induced by Dopamine During Visual Stimulation and Spontaneous Activity

We next explored how oscillations in different LFP-bands are affected by DA. Because the effect of neuromodulation on V1 likely depends on the operational mode of the network, we examined the LFP-spectrum under systemic injection of L-DOPA, either without stimulus presentation (Spontaneous; Figure 3A-C top panels) or while presenting movie clips (Movie; Figure 3A-C bottom panels). Since different cortical layers show distinct patterns of connectivity, physiology and sensory responses [29, 40, 41], we quantified the effect of DAergic neuromodulation separately on the LFP spectrum recorded in each of three laminar compartments (SG, G and IG).

We observed profound changes in V1 LFP-power during injection of L-DOPA compared to before the injection (Figure 3), that depended on cortical depth and frequency, and differed between movie-evoked and spontaneous activity. We quantified the changes in power after L-DOPA injection by normalizing the power of each LFP band so that its value, averaged across trials and time points in the 12-min period preceding the injection, was set to 1.

We first considered the effect of L-DOPA during spontaneous activity. During L-DOPA injection, the spontaneous LFP power increased prominently in the nMOD-band (Figure 3A-C, top panel), while it decreased in the γ-band (50–150 Hz; Figure 3A-C, top panel). These effects were very prominent in the SG layers (nMOD: averaged normalized power=1.73±0.12, t-test p=0.021; γ: 0.53±0.08, t-test p=0.038) and were also large in IG layers (nMOD: averaged normalized power=1.45±0.08, t-test p=0.035; γ: 0.53±0.07, t-test p=0.026). (Here and hereafter, results are reported as mean ± sem across all available channels in all sessions in the specified laminar compartment, unless otherwise stated). Modulation of both nMOD and γ

during L-DOPA injection was also present, but less prominent, in the G layers (nMOD: average normalized power=1.22±0.04, p=0.041 t-test; γ: 0.085±0.03, p-0.048 paired t-test). The power of the α band was less modulated by DA than that of other bands (Figure 3A-C), with the largest DA modulation in SG (average normalized power=1.21±0.04, p=0.043, paired t-test). The band-specific changes in spontaneous power discussed above were confirmed by repeating the same analysis using the power of individual Fourier coefficients (Figure 3A-C, bottom panels). This finer analysis confirmed the band-specific results, in particular indicating a strong increase in power in the 19–38 Hz range and a strong decrease in power in the 50–150 Hz range in the SG and IG layers (Figure 3A-C, bottom panels).

We then considered the power changes induced by injection of L-DOPA during movie stimulation (Figure 3D-F). There was a significant increase in nMOD movie-evoked power in SG (p=0.028, paired t-test), and IG layers (p=0.033, paired t-test), but not in the G layers (p =0.058, paired t-test). However, and in sharp contrast to spontaneous activity, the movie-evoked γ-power in all cortical layers significantly increased during the injection (SG: p=0.024; IG: p=0.031; G: p=0.032, paired t-test; Figure 3D-F, bottom panel).

In the post-injection recovery phase, all bands returned to baseline both during spontaneous and movie-evoked activity; however, the return to baseline appeared slower in the nMOD and α bands (Figure 3C,F), suggesting that systemic injection of L-DOPA has a particularly prolonged effect on these bands.

In summary, these results suggest that DA elicits LFP-power changes in V1 that were not only strongly frequency- and layer-specific, but also profoundly differed depending on whether or not the V1 network was processing a visual stimulus. This highlights the strong dependence of the effect of DA neuromodulation on the operational state of the network.

Layer and Frequency Specific Changes in Information Induced by Dopamine

To address directly the effect of DA on the information carried by different frequency oscillations in different laminae, we computed the information carried by the power at each frequency about which movie scene was being presented (Eq. 2, STAR Methods) before, during and after L-DOPA injection (Figure 4).

We first considered the laminar profile of the information carried before L-DOPA injection. We found (Figure 4A) that the γ and high-γ bands reached maximal information about the movie in the SG layers. γ and high-γ bands had much lower information in the G layers and IG layers. The α band showed a less pronounced laminar dependence than γ and high-γ. The nMOD power carried little information about the movie across all layers, with little laminar dependence. These results were confirmed by the individual Fourier coefficient analysis, which showed high information in the SG for all individual frequencies in the high frequency range (50–150 Hz, covering γ and high-γ ranges, Figure 4B, "Before"). In addition, the information in all individual frequencies below 50 Hz was lower and less layer-dependent than the information in the frequencies above 50 Hz. Moreover, the information in all the frequencies within the nMOD range was low in all layers, thereby confirming the results of the analysis of discrete frequency bands.

We then tested the effect of L-DOPA injection on the frequency- and layer-specific distribution of information (Figure 4A). We found that during L-DOPA injection there was an increase in information about the movie across a wide spectrum of frequencies and cortical depths. This increase was particularly pronounced in the SG layers, where it was significant for all bands and especially noticeable for the γ and nMOD bands (values before and after L-DOPA injection: γ: 0.24±0.021 vs 0.34±0.02 bits, p=0.031; high-γ: 0.23±0.015 bits vs 0.32±0.021 bits, p=0.021; α: 0.14±0.018 vs 0.22±0.021 bits, p=0.013; nMOD: 0.04±0.03 vs 0.15±0.02, and p=0.039; all paired t-tests). In the G layers, the increase in information during L-DOPA injection was significant for the α band (p=0.031). In the IG layers, the increase in movie information

after L-DOPA injection was significant for nMOD (0.10±0.03 bits, p=0.043), γ and high-γ (0.30±0.04 bits, p=0.045; and 0.23±0.02 bits, p=0.037, respectively, see Figure 3).

The DA-induced effects on the selected frequency bands and cortical layers were also confirmed when considering individual Fourier coefficients and electrode locations (Figure 4B, "Before" vs "During" periods). We also observed that the information about the movie remained high following the end of the injections (Figure 4B, "After" period). In particular, we observed that the information in the γ and high-γ bands remained high compared to the pre-injection period in the SG and IG layers. However, in the G layers we observed higher, longer-lasting information in the post-injection period only for the α band.

Importantly, both information and power provided different perspectives to the data. This is demonstrated in Supplemental Information (Figure S1D-F) where we report that power and information correlate only within specific frequency bands and that changes in power with L-DOPA injection do not correlate with the changes in information.

Dopamine-Induced Changes in LFP Oscillation Variability

The amount of information about the movie carried by the LFP power depends on both the signal (that is, how strongly the trial-averaged LFP response changes across different movie scenes) and the noise (that is, how strong is the variability in the LFP power fluctuations to repeated presentations of the same movie scene, Eq. 3, STAR Methods). The changes in information caused by the injection of L-DOPA may thus be attributable to a higher signal, to lower noise, or both. We address this question by quantifying, independently for each frequency, the changes in the signal and noise after L-DOPA injection. We computed the signal, as the coefficient of variation (CV) across different scenes of the movie of the trial-averaged evoked LFP power in each scene ("signalCV"; Eq. 4, STAR Methods; solid lines in Figure 5). Furthermore, we quantified the noise as the CV over trials of the variations of the power evoked by each scene around its scene-specific trial-average value, then averaged over all scenes ("noiseCV"; Eq. 5, STAR Methods; dashed lines in Figure 5).

We first considered the distribution of signal and noise across layers before L-DOPA injection (Figure 5A). In agreement with a previous study that did not record layer specific changes [6], we found that on average, across layers, the γ and high-γ band contained more information because they had both a high signalCV and low noiseCV. More specifically, the γ band had the highest signalCV (peaking at 0.31±0.04 at 99±4 Hz) and the lowest noiseCV (dipping at 0.64±0.05 at ~55 Hz). Frequencies in the nMOD-band had the lowest signal (0.09±0.01) and a particularly high noiseCV (0.88±0.02), which explains why little information was seen in this band. These patterns were also noticeable in the visual inspection of individual traces of these bands (Figure S3).

Given that our results indicate that information is not uniformly distributed across layers (Figure 4B), we quantified whether such pre-injection laminar information profiles can be ascribed to differences in the signal or noise from the different layers. We computed the signal and noise variability from each cortical layer before L-DOPA injection (Figure 5B). We found that LFPs in SG layers tended to have more signal than other layers across a wide frequency spectrum (covering the α band; p=0.035, but especially prominent in γ and high-γ bands; p=0.031 and p=0.035) and less noise specifically in the γ and high-γ bands (Figure 5B, p=0.038 and p=0.042).

We then considered how DA affected the noise and signal across cortical layers and frequency bands (Figure 5C), by considering responses collected during the injection of L-DOPA. Injection of L-DOPA tended to increase signal and decrease noise across a wide range of frequencies in a layer-dependent fashion. In particular, we observed a particularly marked effect in SG and IG layers (Figure 5C). In the SG layers, the maximal increase of signalCV due to L-DOPA injection was 0.43±0.03 at 105 Hz, and maximal decrease of noiseCV was 0.64±0.02 at 75 Hz). More specifically, injection of L-DOPA increased the signalCV over a wide frequency range including nMOD, γ and high-γ bands in SG and IG layers (Figure 5C). The injections of L-DOPA also decreased the noise throughout the spectrum in the α, nMOD,

γ and high-γ bands in SG layers, and decreased the noise in the nMOD, γ and high-γ bands in IG layers (Figure 5C).

In contrast to the DA-induced increase of signal and noise variance in SG and IG layers over a wide range of frequencies, the variance of the signal and noise in the G layers did not change much after injection of L-DOPA, which further supports the idea that information processing in this layer is much less affected by DA.

Layer Dependent Changes in the Correlations Between LFP Powers at Different Frequencies

Another important question is whether DA changes the relationship between oscillations in different bands [10, 42]. We distinguished between two possible types of correlations between the power in different bands. The first is signal correlation, which quantifies the similarity of stimulus preferences between the power at different frequencies, and is defined as the Pearson correlation between the trial-averaged power at the two frequencies in response to each movie scene [6, 42, 43]. The second is noise correlation, which quantifies the correlation in neural activity not due to stimulus covariation, and is defined here as the Pearson correlation between the trial-to-trial fluctuations around their across-trial average of power at the two frequencies for each movie scene [6, 42, 43].

Figure 6 shows the average signal correlation over the entire dataset for different frequencies and cortical depths, before and during L-DOPA injection, for individual frequencies (Figure 6A) and band-limited data (Figure 6B). Before the injection, the signal correlation was highest in the γ-band, and was also high in the high-γ and α band. Signal correlations were much smaller for the nMOD-band. Signal correlations across bands were smaller than those within the same band (Figure 6A-B). The most prominent effect of L-DOPA injection was to greatly increase the signal correlations (and thus the similarity of stimulus preferences of the response at different frequencies) in the γ and high-γ range. In the γ-band, the increase due to DA was pronounced and significant ($p < 0.05$; paired t-test) in each layer (Figure 6B). The γ-band signal

correlation after DA injection was higher in SG and IG than the signal correlation before and during L-DOPA injection ($p< 0.05$ in all layers). An increase in within-band signal correlation during injection was also found for the α band, particularly for the SG ($p=0.032$) and IG ($p=0.035$) layers, but not in the nMOD-band.

We also observed that changes in DA increased the signal correlations between different bands. The pairwise correlations between frequencies in the α- and nMOD-bands increased in both the SG and the G layers during injection ($p=0.03$). In addition, the correlations between α and γ increased ($p=0.03$) in all layers.

In summary, as well as increasing the amount of information over a wide range of oscillation frequencies, L-DOPA injection made different frequency ranges respond more similarly to different stimuli, as DA increased signal correlations across frequencies, particularly in the SG and IG layers.

One possibility is that the increased similarity of the stimulus tuning of different frequency bands with L-DOPA injection is due to individual frequency bands becoming wider and thus overlapping more. If that were the main reason for a signal correlation increase, we would expect to also observe an increase in noise correlation across frequency bands during L-DOPA injection. However, we found that noise correlation did not change in any band at any depth during injection (Figure S4). Also, correlations among frequencies during spontaneous activity did not change during L-DOPA injection (Figure S5).

DISCUSSION

Neuromodulation gives neural circuits the flexibility to dynamically reconfigure their activity to meet cognitive demands. Here we investigated how neuromodulation affects the power and information content of oscillatory activity, an aspect of neural activity thought to be central to cortical information processing. By recording neural activity in different cortical layers of V1 in anesthetized monkeys, and pharmacologically mimicking DAergic neuromodulation, we

demonstrated that the power of middle-frequency endogenous oscillations correlates with the DA levels. Furthermore, we demonstrated that an increase in the level of DA significantly enhances the sensory information content over a wide range of frequencies, but it especially increases the information in the γ-frequencies in the cortical output layers.

Endogenous Middle-Frequency [19–38 Hz] Oscillations as Marker of Dopaminergic Neuromodulation

Tracking changes of neuromodulators over time and in individual trials is important to establish how neuromodulators dynamically regulate cortical computations and shape cognitive functions such as learning and attention. It is also crucial to understand how dysfunction of neuromodulatory systems may lead to disorder-specific abnormalities of cortical oscillations. Since in many experiments only cortical recordings are available because neuromodulatory nuclei are difficult to record from, it is important to discover statistical markers of changes in neuromodulation in cortical activity. We found that the power of the [19–38 Hz] band was the most accurate statistical marker of the level of DA, because it increased in power when DA was pharmacologically increased, both during spontaneous activity and during visual stimulation. Our statistical analysis also confirmed [6, 31] that this band was only weakly modulated by external stimuli, that all frequencies in this band strongly co-varied according to non-stimulus-driven factors, and that have weak correlation with the power of other bands. Together, these facts allow us to ascribe changes in this frequency band to changes in an internal state driven by DA. These findings suggest the [19–38 Hz] band can, at least in V1, be rightfully termed a neuromodulatory band, and that it can be used to statistically infer that changes in its neural activity reflect changes in DA levels. Importantly, the LFP correlates well with surface EEGs [5]. This suggests that pre-stimulus fluctuations in power in occipital EEGs in the mid-frequency band may be used to track fluctuations of DA.

Our findings fit well with earlier studies suggesting that mid-frequency power modulation reflects endogenous, not stimulus-modulated, neural activity [5, 6, 44-49], which are associated to maintenance of the current cognitive state. However, a novelty of our study is to

show that the power of this band is DA-related. Given that other cortical regions have higher concentration of DA receptors than V1, it is thus natural to suggest that [19–38 Hz] power changes over other cortical regions may reflect fluctuations in the concentration of neuromodulators [2, 45, 50]. Further studies are needed to establish how these DA-mediated effects may interact with other neuromodulators, such acetylcholine, which may have complex, and sometimes opposite, effects on different frequency bands [51].

Given that V1 lacks DA-receptors [16, 17], one question regards how these power modulations arise in V1 and why do they cover the [19–38 Hz] frequency range. Oscillations in neural systems often arise because of closed loop interactions between factors increasing and decreasing neural activity [52]. The period of the oscillation depends on the number of steps in the loop and on the time scales of each factor [53]. Frequencies in the γ-range are generated by local loops between excitatory and inhibitory neurons involving only a very small number of synaptic steps [53]; thus the slower nMOD oscillations may be generated by feedback loops involving more step and/or slower factors, possibly involving both basal ganglia feeding to visual cortex [54, 55], or higher order areas of cortex, endowed with DA-receptors, feeding back to visual cortex [19, 20, 22].

A caveat of these results, to be addressed with further studies, is that it is unknown whether the concentrations of DA in the anesthetized condition differ from those of awake animals. To minimize this concern, we chose an anaesthesia protocol (see STAR Methods) that targets μ-opioid receptors with low densities in regions, such as ventral tegmental area, substantia nigra and frontal regions [56], more involved with release and reception of DA. Therefore, levels of DA are likely to be only mildly affected by our anaesthesia. Indeed, studies comparing awake and anaesthetized neurovascular coupling suggest that our anaesthesia protocol does not affect much fMRI and neurophysiological responses in visual cortices [18, 57, 58].

Layer and Frequency Dependent Increase of Information due to Dopamine

We found that while DA in general increased visual information, these gains were strongly layer and frequency dependent. The most notable effect was that DA markedly increased the information of the γ-band in the SG and lG layers. Gamma oscillations have been implicated in the dynamic transmission of information along feedforward pathways [8, 59], and neurons that send feedforward projections to higher cortical areas are located in the SG layers [60]. This suggests that the DA-mediated increase in γ information in SG may be a mechanism to increase the efficiency of feedforward propagation of sensory information to higher areas [8, 19, 22]. Enhancing the readout of task-related information is a function often attributed to DA [22, 61-64], and thought to be mediated by DA increasing the signal-to-noise ratio of sensory representation in frontal areas [19, 22, 65, 66]. Our results, hence, are compatible with the general idea that DA promotes the cortical flow and readout of sensory information, and add the new perspective that it may do so by improving the feedforward transmission of early cortical information.

Although DA increased the α band information in the SG and G layers, the α band information showed a laminar pattern of low information values that was only very slightly changed by DA. Recent studies proposed that α mediates top-down information flow [8, 26]. Although the small DA-induced increase in α band information may reflect how DA improves cortico-cortical communication from higher areas to V1 [8, 18, 19], a caveat of our results is that DA-related changes in α information may be larger in awake subjects performing cognitive tasks requiring top down information [9, 28, 64] than in our anaesthetized data.

Shared Sources of Signals Between nMOD and the Other Bands

We found that changes in the levels of DA also increased the signal correlations, i.e., the similarity in the tuning of different frequency bands to different movie scenes. Given that we also found that DA did not change the noise correlations, the effect of an increase in signal correlation is to increase the redundancy of the information carried by each band. We

speculate that this enhanced redundancy could facilitate the behavioral readout of the visual features. This would fit with theories suggesting that the extraction and amplification of specific sensory features, whose high behavioral relevance has been established by reinforcement learning, is orchestrated in a layer-dependent way by DA [62].

Concluding statement

Our study suggests that dopamine has a profound effect in enhancing and shaping the information content of oscillatory activity in V1. In particular, the DA-mediated layer-dependent increase of information in the γ-band may be a key mechanism promoting the readout of sensory information and improving behavioral performance. Moreover, we found that endogenous cortical oscillations in the [19–38 Hz] band increase with dopamine, suggesting that these oscillations could be used to track changes elicited by dopamine on cortical activity over time or across trials of cognitive tasks.

406 ## AUTHOR CONTRIBUTIONS

407 Conceived the study: DZ, SP. Performed the study: DZ. Analyzed data: DZ with contributions
408 of SCL. Interpreted Results: DZ, SP. Provided materials and methods: DZ, JG, SCL, NKL, SP.
409 Wrote the paper: DZ, SP. Edited the paper and commented on it: JG, SL, NKL.

410 ## ACKNOWLEDGMENTS

411 We thank Deniz Ipek, Ulrike Passlack and Mirko Linding for their technical assistance, and
412 John Assad and Allison Hamilos for useful comments on an earlier version of this manuscript.

413

REFERENCES

1. Marder, E., O'Leary, T., and Shruti, S. (2014). Neuromodulation of circuits with variable parameters: single neurons and small circuits reveal principles of state-dependent and robust neuromodulation. Annu Rev Neurosci *37*, 329-346.

2. Dayan, P. (2012). Twenty-five lessons from computational neuromodulation. Neuron *76*, 240-256.

3. Uhlhaas, P.J., and Singer, W. (2015). Oscillations and neuronal dynamics in schizophrenia: the search for basic symptoms and translational opportunities. Biol Psychiatry *77*, 1001-1009.

4. Buzsaki, G., and Draguhn, A. (2004). Neuronal oscillations in cortical networks. Science *304*, 1926-1929.

5. Whittingstall, K., and Logothetis, N.K. (2009). Frequency-band coupling in surface EEG reflects spiking activity in monkey visual cortex. Neuron *64*, 281-289.

6. Belitski, A., Gretton, A., Magri, C., Murayama, Y., Montemurro, M.A., Logothetis, N.K., and Panzeri, S. (2008). Low-frequency local field potentials and spikes in primary visual cortex convey independent visual information. J Neurosci *28*, 5696-5709.

7. Schroeder, C.E., and Lakatos, P. (2009). Low-frequency neuronal oscillations as instruments of sensory selection. Trends Neurosci *32*, 9-18.

8. van Kerkoerle, T., Self, M.W., Dagnino, B., Gariel-Mathis, M.A., Poort, J., van der Togt, C., and Roelfsema, P.R. (2014). Alpha and gamma oscillations characterize feedback and feedforward processing in monkey visual cortex. Proc Natl Acad Sci U S A *111*, 14332-14341.

9. van Kerkoerle, T., Self, M.W., and Roelfsema, P.R. (2017). Layer-specificity in the effects of attention and working memory on activity in primary visual cortex. Nat Commun *8*, 13804.

10. Einevoll, G.T., Kayser, C., Logothetis, N.K., and Panzeri, S. (2013). Modelling and analysis of local field potentials for studying the function of cortical circuits. Nat Rev Neurosci *14*, 770-785.

11. Logothetis, N.K. (2008). What we can do and what we cannot do with fMRI. Nature *453*, 869-878.

12. Uhlhaas, P.J., and Singer, W. (2010). Abnormal neural oscillations and synchrony in schizophrenia. Nat Rev Neurosci *11*, 100-113.

13. Holroyd, S., and Wooten, G.F. (2006). Preliminary fMRI evidence of visual system dysfunction in Parkinson's disease patients with visual hallucinations. J Neuropsych Clin N *18*, 402-404.

14. Algaze, A., Leguire, L.E., Roberts, C., Ibinson, J.W., Lewis, J.R., and Rogers, G. (2005). The effects of L-dopa on the functional magnetic resonance imaging response of patients with amblyopia: a pilot study. J AAPOS *9*, 216-223.

15. Rogers, G.L. (2003). Functional magnetic resonance imaging (fMRI) and effects of L-dopa on visual function in normal and amblyopic subjects. Trans Am Ophthalmol Soc *101*, 401-415.

16. Lidow, M.S., Goldman-Rakic, P.S., Gallager, D.W., and Rakic, P. (1991). Distribution of dopaminergic receptors in the primate cerebral cortex: quantitative autoradiographic analysis using [3H]raclopride, [3H]spiperone and [3H]SCH23390. Neuroscience *40*, 657-671.

17. Lidow, M.S., Goldman-Rakic, P.S., Rakic, P., and Gallager, D.W. (1990). Autoradiographic comparison of D1-specific binding of [3H]SCH39166 and [3H]SCH23390 in the primate cerebral cortex. Brain Res *537*, 349-354.

18. Zaldivar, D., Rauch, A., Whittingstall, K., Logothetis, N.K., and Goense, J. (2014). Dopamine-induced dissociation of BOLD and neural activity in macaque visual cortex. Curr Biol *24*, 2805-2811.

19. Noudoost, B., and Moore, T. (2011). Control of visual cortical signals by prefrontal dopamine. Nature *474*, 372-375.

20. Moore, T., and Zirnsak, M. (2017). Neural Mechanisms of Selective Visual Attention. Annu Rev Psychol *68*, 47-72.

21. Happel, M.F. (2016). Dopaminergic impact on local and global cortical circuit processing during learning. Behav Brain Res *299*, 32-41.

22. Jacob, S.N., Ott, T., and Nieder, A. (2013). Dopamine regulates two classes of primate prefrontal neurons that represent sensory signals. J Neurosci *33*, 13724-13734.

23. Mitzdorf, U., and Singer, W. (1979). Excitatory synaptic ensemble properties in the visual cortex of the macaque monkey: a current source density analysis of electrically evoked potentials. The Journal of comparative neurology *187*, 71-83.

24. Maier, A., Adams, G.K., Aura, C., and Leopold, D.A. (2010). Distinct superficial and deep laminar domains of activity in the visual cortex during rest and stimulation. Front Syst Neurosci *4*.

25. Pettersen, K.H., Devor, A., Ulbert, I., Dale, A.M., and Einevoll, G.T. (2006). Current-source density estimation based on inversion of electrostatic forward solution: effects of finite extent of neuronal activity and conductivity discontinuities. J Neurosci Methods *154*, 116-133.

26. Dougherty, K., Cox, M.A., Ninomiya, T., Leopold, D.A., and Maier, A. (2017). Ongoing Alpha Activity in V1 Regulates Visually Driven Spiking Responses. Cereb Cortex *27*, 1113-1124.

27. Maier, A., Aura, C.J., and Leopold, D.A. (2011). Infragranular sources of sustained local field potential responses in macaque primary visual cortex. J Neurosci *31*, 1971-1980.

28. Self, M.W., van Kerkoerle, T., Super, H., and Roelfsema, P.R. (2013). Distinct roles of the cortical layers of area V1 in figure-ground segregation. Curr Biol *23*, 2121-2129.

494 29. Lund, J.S. (1973). Organization of neurons in the visual cortex, area 17, of the
495 monkey (Macaca mulatta). The Journal of comparative neurology *147*, 455-496.

496 30. O'Kusky, J., and Colonnier, M. (1982). A laminar analysis of the number of neurons,
497 glia, and synapses in the adult cortex (area 17) of adult macaque monkeys. The
498 Journal of comparative neurology *210*, 278-290.

499 31. Belitski, A., Panzeri, S., Magri, C., Logothetis, N.K., and Kayser, C. (2010). Sensory
500 information in local field potentials and spikes from visual and auditory cortices: time
501 scales and frequency bands. J Comput Neurosci *29*, 533-545.

502 32. Szymanski, F.D., Rabinowitz, N.C., Magri, C., Panzeri, S., and Schnupp, J.W.
503 (2011). The laminar and temporal structure of stimulus information in the phase of
504 field potentials of auditory cortex. J Neurosci *31*, 15787-15801.

505 33. Zaldivar, D., Logothetis, N.K., Rauch, A., and Goense, J. (2017). Pharmaco-Based
506 fMRI and Neurophysiology in Non-Human Primates. In In Vivo Neuropharmacology
507 and Neurophysiology, A. Philippu, ed. (New York, NY: Springer New York), pp. 37-
508 66.

509 34. Black, K.J., Carl, J.L., Hartlein, J.M., Warren, S.L., Hershey, T., and Perlmutter, J.S.
510 (2003). Rapid intravenous loading of levodopa for human research: clinical results. J
511 Neurosci Methods *127*, 19-29.

512 35. Henrie, J.A., and Shapley, R. (2005). LFP power spectra in V1 cortex: the graded
513 effect of stimulus contrast. J Neurophysiol *94*, 479-490.

514 36. Frien, A., Eckhorn, R., Bauer, R., Woelbern, T., and Gabriel, A. (2000). Fast
515 oscillations display sharper orientation tuning than slower components of the same
516 recordings in striate cortex of the awake monkey. Eur J Neurosci *12*, 1453-1465.

517 37. Quian Quiroga, R., and Panzeri, S. (2009). Extracting information from neuronal
518 populations: information theory and decoding approaches. Nat Rev Neurosci *10*,
519 173-185.

520 38. de Ruyter van Steveninck, R.R., Lewen, G.D., Strong, S.P., Koberle, R., and Bialek,
521 W. (1997). Reproducibility and variability in neural spike trains. Science *275*, 1805-
522 1808.

523 39. Donner, T.H., Siegel, M., Oostenveld, R., Fries, P., Bauer, M., and Engel, A.K.
524 (2007). Population activity in the human dorsal pathway predicts the accuracy of
525 visual motion detection. J Neurophysiol *98*, 345-359.

526 40. Callaway, E.M. (1998). Local circuits in primary visual cortex of the macaque
527 monkey. Annu Rev Neurosci *21*, 47-74.

528 41. Nassi, J.J., and Callaway, E.M. (2009). Parallel processing strategies of the primate
529 visual system. Nat Rev Neurosci *10*, 360-372.

530 42. Averbeck, B.B., Latham, P.E., and Pouget, A. (2006). Neural correlations, population
531 coding and computation. Nature Reviews Neuroscience *7*, 358-366.

532 43. Panzeri, S., Schultz, S.R., Treves, A., and Rolls, E.T. (1999). Correlations and the
533 encoding of information in the nervous system. P Roy Soc B-Biol Sci *266*, 1001-
534 1012.

535 44. Haegens, S., Nacher, V., Hernandez, A., Luna, R., Jensen, O., and Romo, R. (2011).
536 Beta oscillations in the monkey sensorimotor network reflect somatosensory decision
537 making. Proc Natl Acad Sci U S A *108*, 10708-10713.

538 45. Engel, A.K., and Fries, P. (2010). Beta-band oscillations--signalling the status quo?
539 Curr Opin Neurobiol *20*, 156-165.

540 46. Buschman, T.J., and Miller, E.K. (2007). Top-down versus bottom-up control of
541 attention in the prefrontal and posterior parietal cortices. Science *315*, 1860-1862.

542 47. Lundqvist, M., Rose, J., Herman, P., Brincat, S.L., Buschman, T.J., and Miller, E.K.
543 (2016). Gamma and Beta Bursts Underlie Working Memory. Neuron *90*, 152-164.

544 48. Schmiedt, J.T., Maier, A., Fries, P., Saunders, R.C., Leopold, D.A., and Schmid, M.C.
545 (2014). Beta oscillation dynamics in extrastriate cortex after removal of primary visual
546 cortex. J Neurosci *34*, 11857-11864.

547 49. Wrobel, A. (2000). Beta activity: a carrier for visual attention. Acta Neurobiol Exp
548 (Wars) *60*, 247-260.

549 50. Yu, A.J., and Dayan, P. (2005). Uncertainty, neuromodulation, and attention. Neuron
550 *46*, 681-692.

551 51. Deco, G., and Thiele, A. (2009). Attention: oscillations and neuropharmacology. Eur J
552 Neurosci *30*, 347-354.

553 52. Buzsaki, G. (2011). Rhythms of the Brain, Volume 1, (Oxford University Press).

554 53. Brunel, N., and Wang, X.J. (2003). What determines the frequency of fast network
555 oscillations with irregular neural discharges? I. Synaptic dynamics and excitation-
556 inhibition balance. Journal of Neurophysiology *90*, 415-430.

557 54. Garvert, M.M., Friston, K.J., Dolan, R.J., and Garrido, M.I. (2014). Subcortical
558 amygdala pathways enable rapid face processing. Neuroimage *102 Pt 2*, 309-316.

559 55. Duncan, S., and Barrett, L.F. (2007). The role of the amygdala in visual awareness.
560 Trends Cogn Sci *11*, 190-192.

561 56. Henriksen, G., and Willoch, F. (2008). Imaging of opioid receptors in the central
562 nervous system. Brain *131*, 1171-1196.

563 57. Magri, C., Schridde, U., Murayama, Y., Panzeri, S., and Logothetis, N.K. (2012). The
564 amplitude and timing of the BOLD signal reflects the relationship between local field
565 potential power at different frequencies. J Neurosci *32*, 1395-1407.

566 58. Ku, S.P., Tolias, A.S., Logothetis, N.K., and Goense, J. (2011). fMRI of the face-
567 processing network in the ventral temporal lobe of awake and anesthetized
568 macaques. Neuron *70*, 352-362.

59. Bosman, C.A., Schoffelen, J.M., Brunet, N., Oostenveld, R., Bastos, A.M., Womelsdorf, T., Rubehn, B., Stieglitz, T., De Weerd, P., and Fries, P. (2012). Attentional Stimulus Selection through Selective Synchronization between Monkey Visual Areas. Neuron *75*, 875-888.

60. Rockland, K.S., and Pandya, D.N. (1979). Laminar origins and terminations of cortical connections of the occipital lobe in the rhesus monkey. Brain Res *179*, 3-20.

61. de Lafuente, V., and Romo, R. (2011). Dopamine neurons code subjective sensory experience and uncertainty of perceptual decisions. Proc Natl Acad Sci U S A *108*, 19767-19771.

62. Happel, M.F., Deliano, M., Handschuh, J., and Ohl, F.W. (2014). Dopamine-modulated recurrent corticoefferent feedback in primary sensory cortex promotes detection of behaviorally relevant stimuli. J Neurosci *34*, 1234-1247.

63. Sarno, S., de Lafuente, V., Romo, R., and Parga, N. (2017). Dopamine reward prediction error signal codes the temporal evaluation of a perceptual decision report. Proceedings of the National Academy of Sciences.

64. Ekstrom, L.B., Roelfsema, P.R., Arsenault, J.T., Bonmassar, G., and Vanduffel, W. (2008). Bottom-up dependent gating of frontal signals in early visual cortex. Science *321*, 414-417.

65. Tian, J., Huang, R., Cohen, J.Y., Osakada, F., Kobak, D., Machens, C.K., Callaway, E.M., Uchida, N., and Watabe-Uchida, M. (2016). Distributed and Mixed Information in Monosynaptic Inputs to Dopamine Neurons. Neuron *91*, 1374-1389.

66. Durstewitz, D., and Seamans, J.K. (2008). The dual-state theory of prefrontal cortex dopamine function with relevance to catechol-o-methyltransferase genotypes and schizophrenia. Biol Psychiatry *64*, 739-749.

67. Logothetis, N.K., Eschenko, O., Murayama, Y., Augath, M., Steudel, T., Evrard, H.C., Besserve, M., and Oeltermann, A. (2012). Hippocampal-cortical interaction during periods of subcortical silence. Nature *491*, 547-553.

68. Logothetis, N.K., Guggenberger, H., Peled, S., and Pauls, J. (1999). Functional imaging of the monkey brain. Nat Neurosci *2*, 555-562.

69. Shannon, C.E. (1948). A Mathematical Theory of Communication. At&T Tech J *27*, 379-423.

70. Magri, C., Whittingstall, K., Singh, V., Logothetis, N.K., and Panzeri, S. (2009). A toolbox for the fast information analysis of multiple-site LFP, EEG and spike train recordings. BMC Neurosci *10*, 81.

71. Panzeri, S., and Treves, A. (1996). Analytical estimates of limited sampling biases in different information measures. Network-Comp Neural *7*, 87-107.

FIGURE CAPTIONS

Figure. 1. Experimental Design.
(A) Experimental paradigm and design. The stimulus consisted of movie clips of 20 s followed by a 20 s presentation of an isoluminant blank screen. Each experiment consisted of three phases: (1) 12 min recording without pharmacological intervention; (2) 12 min recording with carbidopa preconditioning, which does not affect neural activity and prevents the peripheral conversion of L-DOPA to DA; (3) a 48 min long session in which L-DOPA and carbidopa were injected. **(B)** Multi-contact laminar electrodes were used to record neural activity across the cortical layers. **(C)** Session averaged current source density after the movie onset. The sink polarity inversion was used to identify the G/IG border. **(D)** Session average of the coherence between gamma band LFPs across electrode pairs that is used to confirm the location of the G/IG border. The borders of the IG compartment and cortical thickness were determined from anatomical data in the literature. See also Figure S1 and S2.

Figure. 2. Spectral and Information Properties of LFP.
(A) Power spectrum of the spontaneous LFP (red) and the LFP during movie presentation (black). **(B)** Information about the movie contained in LFP power, as function of frequency. Lines and shaded areas in panels A-B show the mean and s.e.m. over all electrodes and sessions. **(C)** Power spectrum of the temporal modulation of the coarse (> 0.5 cpd) or fine (< 0.5 cpd) spatial features of the movie presented in the experiments. The plot shows an average of these spectra computed at 49 locations covering the movie and each summed over a circular region of 2 degrees diameter resembling the size of a multi-unit receptive field.

Figure. 3. Dopamine Increases nMOD Oscillations and Induces Frequency and Stimulus Specific Power Changes in Other Bands.
Effects of L-DOPA injection on the LFP power as a function of layer and frequency. In each panel, the line plots on the top of the panel show the time course of the average ± sem (over all sessions and all electrodes in the considered laminar compartment) of the normalized power of four bands: alpha (8–12 Hz; green), nMOD (19–38 Hz; red), gamma (50–100 Hz; orange) and high-gamma (101–150 Hz; dark brown). The colorplot at the bottom of each panel reports the mean ± s.e.m. (over all sessions and all electrodes in the considered laminar compartment) of the power spectrum of the LFP before, during and after injection of dopamine as function of frequency. Panels **A-C** show spontaneous power. Panels **D-E** show movie-evoked power. Panels **(A,D)**, panels **(B,E),** and panels **(C,F)** show supragranular, granular, and infragranular recordings, respectively. In all panels, vertical dashed lines indicate the beginning and the end of the systemic L-DOPA infusion.

Figure. 4. Dopamine Increases the Information Content in SG and IG Layers.
(A) Changes in information content in frequency bands (alpha, nMOD, gamma and high-gamma) across supragranular (SG), granular (G) and infragranular (IG) cortical layers, before (blue), during (black) and after (red) DA injection. Bars plot the mean ± s.e.m. over all sessions and electrodes in the considered laminar compartment. **(B)** Information in the power of the LFP before, during, and after injection of dopamine (average over all sessions) as function of frequency and cortical depth. The color plot shows the mean ± s.e.m. over all sessions.

Figure. 5. Layer Dependent Increase in Signal and Noise Variability Induced by Dopamine. **(A)** signalCV (solid line) and noiseCV (dashed line) averaged across all experiments **(B)** Layer specific differences in the session-averaged signalCV and noiseCV: supragranular (SG; green), granular (G; blue) and infragranular (IG; red) layers. **(C)** Effect of DA on the session-averaged signalCV and noiseCV in different cortical layers. The lines and shaded areas indicate the mean and s.e.m. respectively across all sessions and electrodes in the specified laminar compartment.

Figure. 6. Dopamine Increases LFP Signal Correlations Across Frequencies and Layers. **(A)** Average (across all session and electrodes in the specified laminar compartment) of the signal correlations between pairs of LFP frequencies in supragranular (SG), granular (G) and infragranular (IG) layers before and during dopamine injection. **(B)** Mean ± s.e.m. over sessions of the correlations within and between LFP bands across different cortical layers before (lighter color, wider bar) and during (darker color, narrower bar) pharmacological injection. See also Figure S4 and S4.

STAR METHODS

Contact for Reagent and Resource Sharing

Further information and request for resources and reagents should be directed to and will be fulfilled by the Lead Contact, Dr. Daniel Zaldivar (Daniel.Zaldivar@tuebingen.mpg.de).

Experimental Model and Subject Details

Four healthy rhesus macaques (Macaca mulatta), aged 6–12 years and weighing 5–11 kg, participated in this study. We used three females (G11, H09 and G09) and one male (K07). These animals participated in previous studies that combined fMRI, neurophysiology and pharmacology studies [18, 33]. All experimental procedures were performed during the daytime. Animals were socially housed in an enriched environment under daily veterinary care. Weight and food and water intake were monitored on a daily basis in full compliance with the guidelines of the European Community (EUVD 86/609/EEC). All procedures were approved by the RP with the projects KY 04-09 and KY 04-16.

Method Details

Animal Preparation and Anesthesia

The anesthesia protocol for all the experimental procedures has been described previously [18, 67]. Briefly, before each experiment the monkeys were sedated with intramuscular (IM) injections of glycopyrrolate (0.01 $mg \cdot kg^{-1}$) and ketamine (15 $mg \cdot kg^{-1}$). An intravenous (IV) cannula was placed in the saphenous or posterior tibial vein for administration of liquids, medication and anesthetics. After induction with fentanyl (3 $mg \cdot kg^{-1}$), thiopental (5 $mg \cdot kg^{-1}$) and succinylcholine chloride (3 $mg \cdot kg^{-1}$), animals were tracheally intubated (Rusch, Teleflex, USA) and ventilated using a Servo Ventilator 900C (Siemens, Germany) maintaining an end-tidal CO_2 of 33–35 mm Hg and O_2 saturation above 95%. Balanced anesthesia was maintained with remifentanil (0.5–2 $\mu g \cdot kg^{-1} min^{-1}$) and muscle relaxation was achieved with mivacurium chloride (2–6 $mg \cdot kg^{-1} h^{-1}$) to ensure complete paralysis of the eye muscles. The physiological state of the monkey was kept within normal limits throughout the experiment. Body temperature was maintained at 38–39°C. Lactate Ringer's (Jonosteril, Fresenius Kabi,

Germany) with 2.5% glucose was continuously infused at a rate of 10 $ml \cdot kg^{-1} \cdot hr^{-1}$ in order to maintain an adequate acid-base balance and intravascular volume and blood pressure; hydroxyethyl starch (Volulyte, Fresenius Kabi, Germany) was administered as needed.

Remifentanil and mivacurium were stopped prior to the emergence of anesthesia, which typically lasted on average between 30 and 40 min after mivacurium was stopped, and without complication. Once spontaneous respiration was assured and an appropriate muscular tone was assessed, the trachea was extubated. Subsequently, the monkeys were taken to their cage were we monitored their behavior. After each experiment, the monkeys were given a resting period of at least 15 days in which monkeys, in which monkeys were freely moving in their cage and received daily veterinarian care.

Visual Stimulation

Two drops of 1% ophthalmic solution of anticholinergic cyclopentolate hydrochloride was applied into each eye to achieve cycloplegia and mydriasis. The eyes of the monkeys were kept open with custom-made irrigating-lid speculae to prevent drying of the tissue. The speculea irrigated the eyes with saline from the medial and lateral canthus at an infusion rate of 0.07 $ml \cdot min^{-1}$. Refractive errors were measured and hard contact lenses (Wöhlk-Contact-Linsen, Schönkirchen, Germany) were placed on the monkey's eye to focus on the plane on which stimuli are presented.

The visual stimulus was delivered using a PC equipped with two VX113 graphics systems. All image generation was in 24-bit true color, using hardware double buffering to provide smooth animation. The stimulation software was written in C and utilized Microsoft's OpenGL 1.1. We presented binocularly using an in-house custom-built projector (SVGA fiber optic system with a resolution of 800x600 pixels with a 30 Hz frame rate). It is worth noting that, to confirm the results we obtained were not dependent on specific details of the stimulus presentation device used, we repeated the movie presentation experiment (without the dopamine injection, but using the same anesthesia protocol) in n=2 monkeys using a CTR monitor (Iiyama MA203DT

Vision Master Pro 513, frame rate 118 Hz, placed at eye level, 50 cm in front of the eye) and we found a very similar pattern of LFP power and LFP information as function of frequency as the one presented in this paper (data not shown), suggesting that the results presented here were not too sensitive to the stimulus delivery method and the frame rate.

The eyepieces of the stimulus presentation system were positioned and adjusted using a modified fundus camera [Zeiss RC250; see 68]. The visual stimulus consisted of high contrast (100%) gamma corrected, fast-moving, colorful movie clips (no soundtrack) from commercially available movies. Stimulus timing was controlled by a Pentium computer (Advantec) running a real-time OS (QNX-Ottawa, Canada). We induced activity in V1 using a block paradigm consisting: 1) an isoluminant blank screen lasting 20 s; 2) a movie segment lasting 20 s; and 3) an isoluminant blank screen (20 s; spontaneous; Figure 1A). This block design was repeated 48 times, yielding an experiment with a total duration of 48 minutes (Figure 1A). A photodiode attached to a monitor displaying the stimulus presentation was used to ensure accurate control of the timing of stimulus presentation.

Pharmacological Injections

Each experiment (n = 15, 4 animals) consisted of neural recording during which systemic applications of L-DOPA+Carbidopa (L-DOPA) were performed. We used a custom-built pressure operated pump to systemically inject dopamine [for detailed information, see 33]. Briefly, our pressure-operated injection-system consisted of two independent single-stage pressure regulators, each connected to a digital closed-loop electro-pneumatic controller (267 mL capacity, TESCOM, Emerson Electric Co., Germany). Both controllers house two pulse-width-modulated solenoid valves which are connected to a PID-based 16-microprocessor and to a computer running custom written MATLAB software which help controlling pressure and resulting flow and volume. One of the aforementioned valves measure the desired pressure in the inlet (pressure originally set in the computer; set-point) and the other valve detects the actual pressure in the outlet (feedback point). The signals emitted by the valves are compared every 25 ms and based on the pressure difference between the set-point and the feedback-

749 point, the electro-pneumatic controller opens or closes either of the valves to compensate for
750 the pressure difference. The gas at the desired pressure is distributed to the syringe pump
751 (systemic pharmacology) through the outlet-line. The syringe pump consisted of a self-
752 contained double-acting cylinder made of aluminum (bore size 8 mm and 190 mm height).
753 The double-acting cylinders have two gas ports: one on the top and one on the bottom, and
754 allow the cylinder rod to move in or out depending on the gas entry point.

755 The flow and volume were continuously monitored by high precision flowmeters (Sensirion,
756 Switzerland). Preconditioning was done with 1.5 mg/kg Carbidopa diluted in 50 ml phosphate-
757 buffered-saline (PBS) and injected at 1.1 ml/min over a period of 12 minutes. The combined
758 L-DOPA+Carbidopa applications used 2.1 mg/kg + 0.5 mg/kg L-DOPA+Carbidopa, diluted in
759 50 ml PBS and injected at a rate of 1.1 ml/min over 12 min. The PBS solution consisted of
760 NaCl 137 mM, KCl 2.7 mM, Na_2HPO_4 8.1 mM, KH_2PO_4 1.76 mM, and had a pH of 7.35. All
761 chemicals were purchased from Sigma-Aldrich (Schnelldorf, Germany).

762 **Neurophysiology Data Collection**
763 We performed a small skull trepanation (4–5 mm diameter) over the primary visual cortex (V1)
764 based on stereotaxic coordinates. Subsequently, the meninges were carefully dissected layer-
765 wise (~1 mm dissection diameter) under a microscope (Zeiss Opmi MDU/S5, Germany). The
766 laminar electrodes (NeuroNexus Technologies, Ann Arbor, USA) were slowly advanced into
767 the cortex under visual and auditory guidance using a manual micromanipulator (Narashige
768 Group, Japan). The final electrode position was determined based on CSD [25] and coherence
769 analysis [24]. Coherence analysis measures the similarity in the temporal structure of two
770 signals and quantifies the extent to which they are linearly correlated. This improved our
771 estimation of the boundary between deep and middle layers [24]. As a final check, the location
772 of Layer 4 was confirmed by analysis of multi-unit activity (MUA) that identified layers with
773 shortest latency of spiking activity (not shown). Our laminar probes contained 16 contacts on
774 a single shank of 3 mm long and 50 µm thick. The contacts were spaced 150 µm apart, with
775 a recording area of 176 μm^2 each. We used a flattened Ag-wire positioned under the skin as

776 reference [33]. The area around the electrode was filled with a mixture of 0.6% agar dissolved
777 in NaCl 0.9% at pH 7.4 which guaranteed good electrical contact between the ground and the
778 animal. The impedance of the electrode sites was measured before and during the
779 experiments and ranged between 500 and 800 kΩ.

780 ## Quantification and Statistical Analysis

781 ### LFP Filtering

782 The signals were amplified and filtered into a band of 1 Hz to 8 kHz using a multi-channel-
783 processor amplifier system (Alpha-Omega Engineering, Nazareth, Israel) and then digitized
784 at 20.833 kHz with a 16-bit ADC-converter (National Instruments, Austin, TX), ensuring
785 sufficient resolution to capture both local field potentials and spiking activity. The LFPs were
786 extracted from the raw recordings by bandpass filtering the signals between 1 and 150 Hz.
787 First, the sampling rate was reduced from the original of 20,835 Hz to 6945 Hz. It was then
788 bandpass filtered and down-sampled in two steps: first to a sampling rate of 1.5 kHz with a
789 fourth order Butterworth filter (500 Hz cutoff), and then to a rate of 500 Hz using a Kaiser
790 window between frequencies of 1 and 150 Hz, with a sharp transition bandwidth (1 Hz). This
791 two-step procedure was more computationally efficient than a single filtering operation to
792 reach the final sampling rate. The sharp second filter was used to avoid aliasing, without
793 requiring a higher sampling rate attributable to a broad filter transition band, which would
794 increase the computational cost of all subsequent operations. To eliminate phase shifts, both
795 forward and backward filtering were used. The power spectral density (PSD) was computed
796 using 500 ms non-overlapping windows using the multitaper method. Normalized PSDs were
797 obtained by dividing the power at each frequency by the average power during the pre-
798 injection movie presentations at that frequency.

Analysis of spectral properties of the movie

To characterise the dynamics of the visual stimuli presented to the animal, we computed the temporal modulation of the power spectral density (PSD) of spatial features in a typical receptive field (RF), as follows: We first converted the full-color RGB movie into luminance using the luminosity function $\boldsymbol{Y = 0.22R + 0.65G + 0.13B}$. For each of 49 simulated RF locations, spaced in a square grid at 1 degree intervals, we extracted a 224x224 square from the 320x240 pixel movie. The patch was spatially filtered using a two-dimensional, fourth-order Butterworth filter, either low-pass or high-pass (with a cut-off at 0.5 cpd in both cases). Subsequently, we summed the absolute value of the filtered movie signal, within a circular receptive field (2 degrees diameter, a typical size for a V1 multi-unit receptive field) centred at this RF location, providing us with a time series of either coarse (> 0.5 cpd) or fine (<0.5 cpd) spatial RF image features throughout the entire 20 s of the movie presentation. The temporal PSD of these time series was then derived using Welch's method, using a window duration of 4s and 75% overlap between consecutive windows. We then reported in Fig 2C the average PSD over all 49 RF locations.

LFP Coherence Analysis

Coherence is a measure of similarity in the temporal structure of two signals that quantifies the extent to which two signals are related to each other. LFP inter-contact coherence was computed based on previous published methods [24]. Briefly, the LFP coherence was computed as magnitude-squared coherence, $C_{xy}(f)$, using Welch's averaged, modified periodogram method and the equation

$$C_{xy}(f)=\frac{|P_{xy}(f)|^2}{P_{xx}(f)P_{yy}(f)}, \qquad \text{Eq. 1}$$

where $P_{xx}(f)$ and $P_{yy}(f)$ are the power spectral densities of each individual signal $x(t)$ and $y(t)$, and $P_{xy}(f)$ is their cross PSD. The resulting functions denote the degree of signal correspondence, or coupling, as a function of frequency, with 1 indicating perfect

824 correspondence and zero indicating that there is no consistent relationship. All coherence
825 measures were performed by averaging the results computed for overlapping 250 ms epoch
826 and averaged consecutively [for details, see 24].

827 **Statistical Tests**
828 We used two-tailed paired t-tests. For the test involving multiple comparisons, we used the
829 Bonferroni correction of the *p*-value.

830 **Information Theoretic Analysis**
831 To determine how well the LFP power r_f at a certain frequency *f* encodes the visual features
832 in the movie, we first divided the 20s movie presentation time into adjacent, non-overlapping,
833 stimulus windows (or "scenes") *s* of length 250 ms. We then computed the mutual information
834 $I(S;R_f)$ [37, 69] between the stimulus window in the movie and the power at frequency f,

835 $$I(S;R_f)=\sum_s P(s)\sum_{r_f} P(r_f|s)\log_2 \frac{P(r_f|s)}{P(r_f)}, \qquad \text{Eq. 2}$$

836 where $P(s)$ is the probability of presentation of the stimulus window *s* (here equal to the
837 inverse of the total number of stimulus windows), $P(r_f|s)$ is the probability of observing a power
838 r_f at frequency *f* in response to a single trial to stimulus *s*, and $P(r_f)$ is probability of observing
839 power r_f across all trials in response to any stimulus. $I(S;R_f)$ quantifies the reduction of the
840 uncertainty about the stimulus that can be gained from observing, in a single-trial, the power
841 at frequency f. Since we use base-two logarithms, $I(S;R_f)$ is expressed in units of bits; 1 bit
842 of information means that, on average, observation of the neuronal response in one trial
843 reduces the observer's stimulus uncertainty by a factor of two.

844 To estimate the information in Eq. 2 from the LFP power in the real data, we used the
845 information breakdown toolbox [70]. The power across trials at each frequency was discretized
846 into 5 equally populated bins. The binned values were then used to estimate the stimulus LFP
847 power probabilities in Eq. 2. We used the Panzeri-Treves algorithm [71] to estimate and

subtract the bias in information estimates due to limited sampling. We assessed the statistical significance of the information values against a null-hypothesis "bootstrap" distribution of values obtained by pairing at random movie scenes and power of neural responses in each trial, thus effectively removing any relationship between the power at a given frequency and the movie scene eliciting it (bootstrap test).

Signal and noise correlations across different frequencies and layers

We determined which frequencies have related stimulus selectivity, and which have shared sources of stimulus-unrelated variability, by performing a linear analysis of correlation (signal and noise) across frequencies. The signal correlation coefficient was computed for each frequency pair ($f1$ and $f2$) and channel as the Pearson's correlation across stimuli of the trial averaged response [6]. Positive values are an indication that two frequencies have similarities in their stimulus preferences, whereas a zero value indicates that the two frequencies have no relationship in their activity [42, 43].

The noise correlations are defined as covariations in the trial-by-trial fluctuations around the mean response [10, 42]. The noise correlation coefficient was computed for each frequency pair ($\mathrm{nf1}$ and $\mathrm{nf2}$) and channel as the Pearson's correlation across stimuli of the trial-averaged-subtracted power. This quantifies the correlations of the variations around the mean of each trial and stimulus window [6, 42]. Positive values of the noise correlation indicate that when the power of one frequency rises above its mean, the power in the other frequency is also more likely to do so [6].

Coefficient of Variations of Signal and Noise

To separate the contribution of stimulus modulation (signal) and response variability (noise) to the information carried by each frequency, we first characterized the movie-evoked power r_f at frequency f in each stimulus window (that is, the movie scenes into which the movie presentation time was partitioned to compute information) as "signal plus noise" [6, 31, 42] as

$$\mathrm{r_f} = \overline{\mathrm{r_f}} + \mathrm{n_f}, \qquad \text{Eq. 3}$$

where the "signal" $\bar{r}_f$ is the trial-averaged power (the bar denotes the average across trials at fixed stimulus) and the "noise" the trial-by-trial fluctuations n_f of the power around their averaged across trials. We stress that such "noise" does not necessarily reflect only noise in the real sense, but reflects all types of variations at fixed stimulus.

We then computed the coefficient of variation (CV) for the signal and the noise in each channel and frequency, as follows. The $\mathrm{signalCV}$ was defined as the CV of the trial-averaged power across the stimulus windows in the movie,

$$\mathrm{signalCV} = \frac{\mathrm{std}_{stim}(\bar{r}_f)}{\langle \bar{r}_f \rangle_{stim}}, \qquad \text{Eq. 4}$$

where $\langle ... \rangle_{stim}$ and std_{stim} denotes the mean and the standard deviation (SD) over the stimulus windows, respectively.

The noiseCV, quantifying the unreliability of the power across trials, was computed as the CV of the power fluctuations across trials about its mean for each stimulus and frequency,

$$\mathrm{noiseCV} = \left\langle \frac{\mathrm{std}_{stim}(n_f)}{\bar{r}_f} \right\rangle_{stim}, \qquad \text{Eq. 5}$$

where std_{stim} denotes the SD across trials at fixed stimulus window.

Data and Software Availability

Analysis-specific code and data are available by request to the Lead Contact.

KEY RESOURCES TABLE

KEY RESOURCES TABLE

REAGENT or RESOURCE	SOURCE	IDENTIFIER
Experimental Models: Organisms/Strain		
Rhesus Macaque (Macaca mulatta)	German Primate Center & Simian Laboratory Europe	N/A NA
Chemicals		
L-DOPA	Sigma-Aldrich	Cat#0400000
Carbidopa	Sigma-Aldrich	Cat#C0460000
NaCl	Sigma-Aldrich	Cat# S6150
KCl	Sigma-Aldrich	Cat# P9333
Na_2HPO_4	Sigma-Aldrich	Cat# NIST2186
KH_2PO_4	Sigma-Aldrich	Cat# P5655
$CaCl_2$	Sigma-Aldrich	Cat# C5670
$MgCl_2$	Sigma-Aldrich	Cat# D9785
Ringer's lactate (Jonosteril)	Fresenius Kabi	N/A
Mivacurium	GlaxoSmithKline (GSK)	Cat# 31178.01.00
Cyclopentolate Hydrochloride	Alcon	Cat#6150277.01.00
Glycopyrrolate	Riemser	Cat#6739722.00.00
Ketamine	WDT, Das Tierarztunternehmen	Cat#9089.01.00
Fentanyl	Janssen	Cat#676282.01.00
Thiopental	Inresa	Cat#6173485.00.00
Succinylcholine chloride	Takeda	Cat#6428407.00.00
Pressure-Operated Pharmacology-System		
Injection System: Digital closed loop (ER5000) electropneumatic controller	TESCOM	http://www.emerson.com/en-us/automation/tescom
Fused Silica Tubes	Technical Glass Products	http://www.technicalglass.com/index.html
Injection System: Liquid flow sensors (SLx –Standalone Liquid Flow Meters)	Sensorion	https://www.sensirion.com/
Critical Commercial Devices		
Servo Ventilator 900C	SIEMENS	https://www.siemens.com/global/en/home.html
Endotracheal Tubus	Teleflex	http://www.teleflex.com
Hard contact lenses	Wöhlk-Contact-Linsen	http://www.linsenpate.de
Trapezoid Diamond Knife	Storzeye	https://www.storzeye.com
Software and Algorithms		
MATLAB	MathWorks	https://www.mathworks.com
Information Toolbox	Magri, et al. 2009	https://github.com/selimonat/InformationBreakdownToolbox
Other		
Multichannel microelectrode arrays (Laminar Probes)	Neuronexus	https://neuronexus.com
Multichannel data system	Alpha-Omega	https://www.alphaomega-eng.com
16-bit ADC converter	National Instruments	http://www.ni.com/de-de.html

Figure1

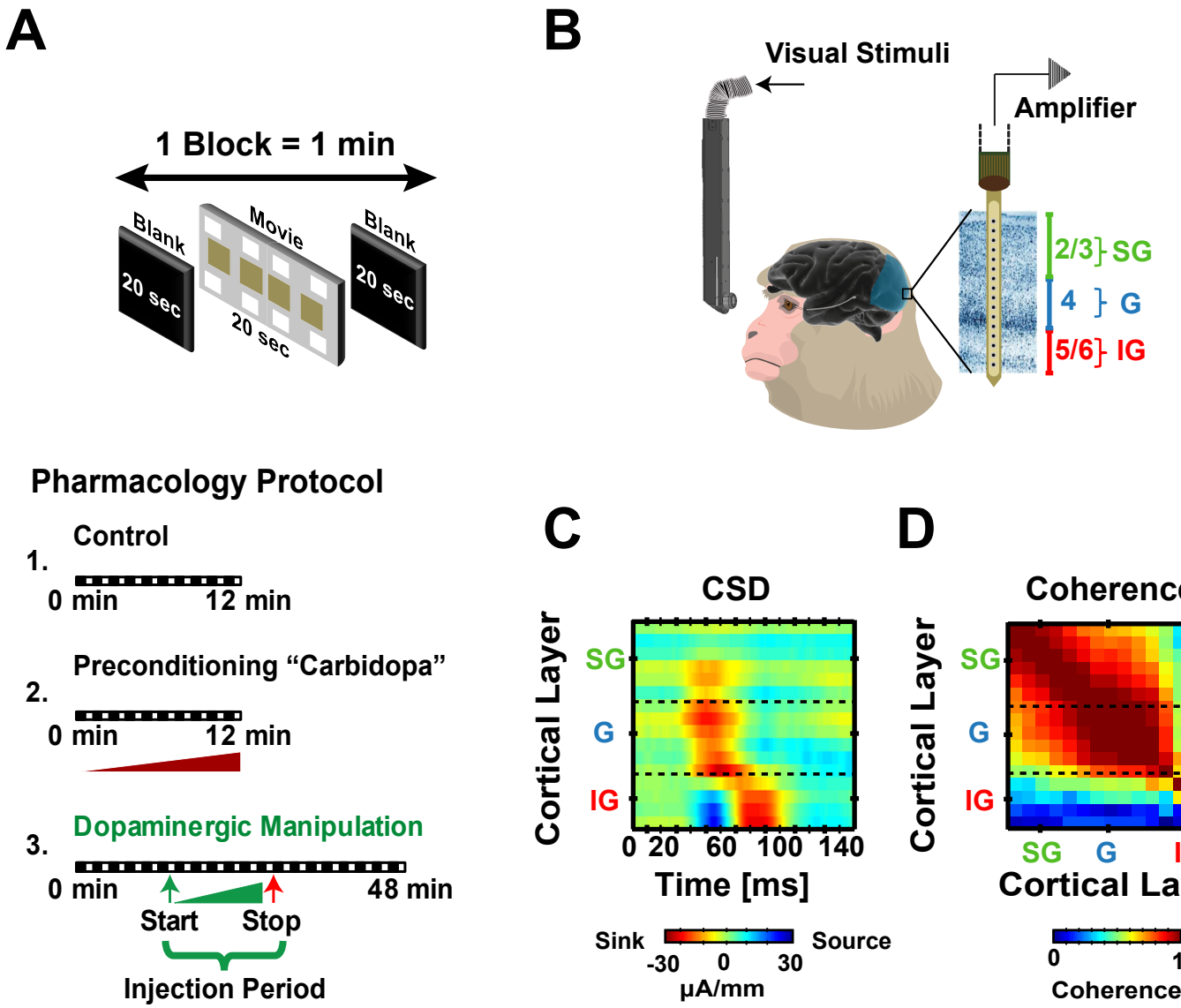
A
1 Block = 1 min
Blank
20 sec
Movie
20 sec
Blank
20 sec
Pharmacology Protocol
1.
Control
0 min
12 min
2.
Preconditioning “Carbidopa”
0 min
12 min
3.
Dopaminergic Manipulation
0 min
48 min
Start
Stop
Injection Period
B
Visual Stimuli
Amplifier
2/3
SG
4
G
5/6
IG
C
CSD
Cortical Layer
SG
G
IG
0 20 60 100 140
Time [ms]
Sink
Source
-30 0 30
μA/mm
D
Coherence
Cortical Layer
SG
G
IG
SG G IG
Cortical Layer
0
1
Coherence

Figure2

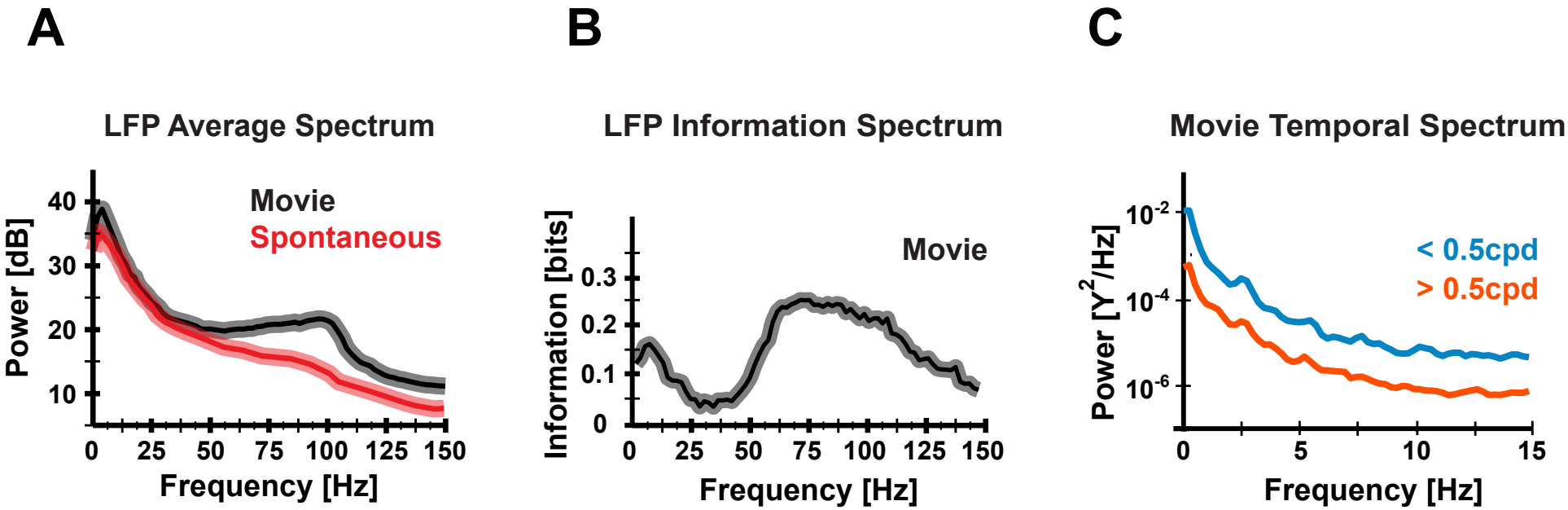
A
LFP Average Spectrum
Movie
Spontaneous
Power [dB]
40
30
20
10
0
25
50
75
100
125
150
Frequency [Hz]
B
LFP Information Spectrum
Movie
Information [bits]
0.3
0.2
0.1
0
0
25
50
75
100
125
150
Frequency [Hz]
C
Movie Temporal Spectrum
< 0.5cpd
> 0.5cpd
Power [Y²/Hz]
10⁻²
10⁻⁴
10⁻⁶
0
5
10
15
Frequency [Hz]

Figure3

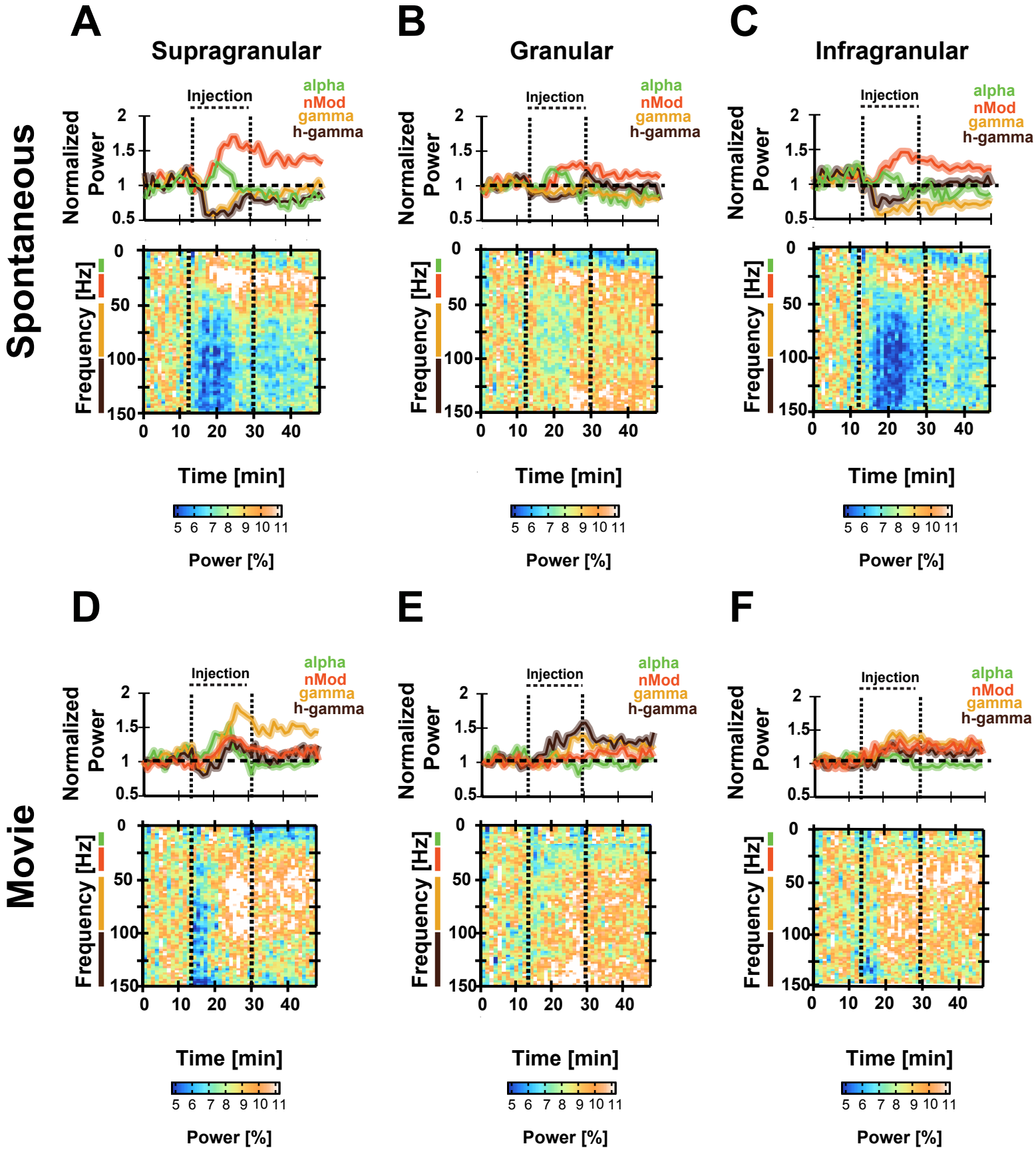
A
Supragranular
B
Granular
C
Infragranular
Spontaneous
Movie
Injection
alpha
nMod
gamma
h-gamma
Normalized Power
Frequency [Hz]
Time [min]
Power [%]
5 6 7 8 9 10 11
D
E
F

Figure4

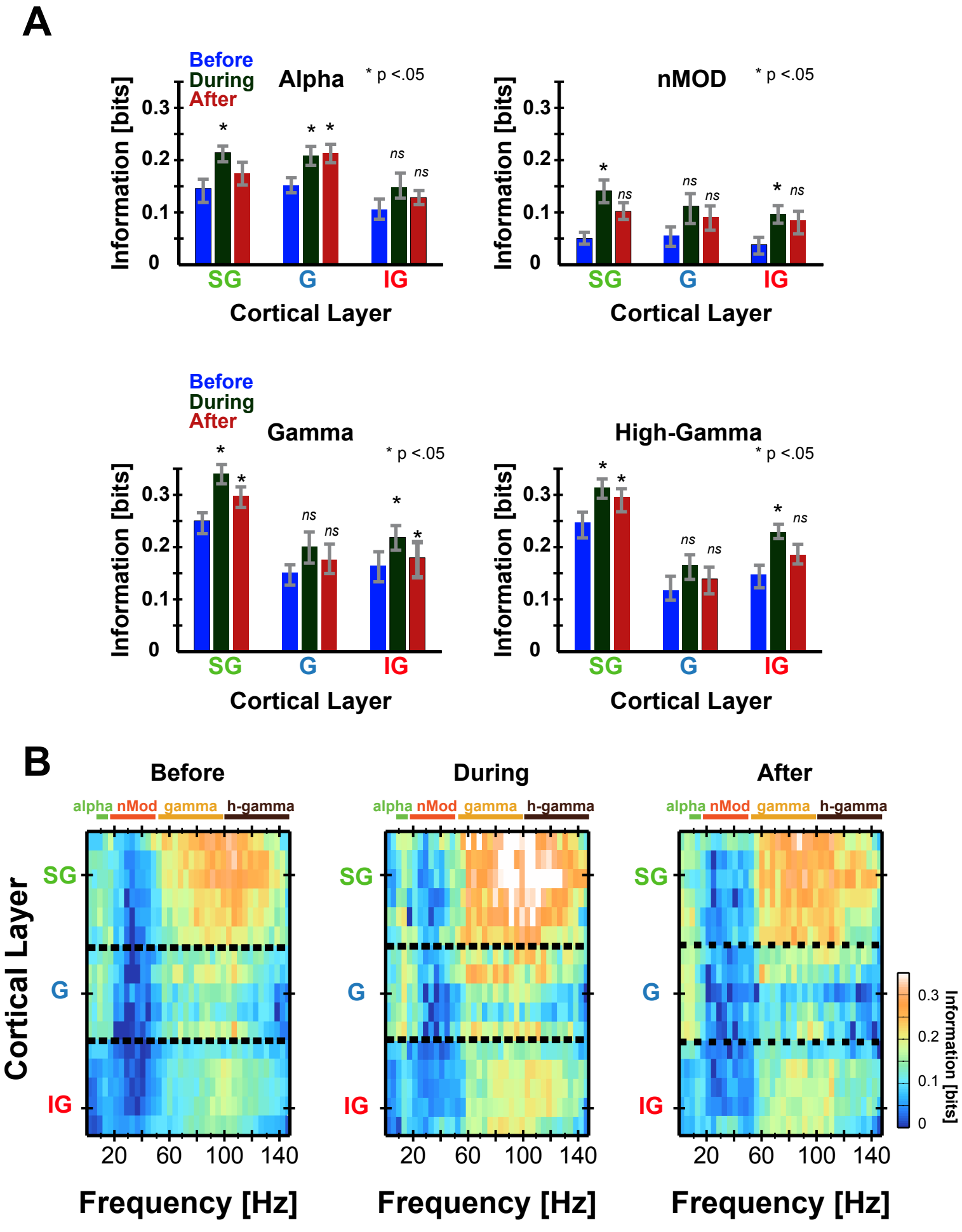
A
Before
During
After
Alpha
* p <.05
nMOD
Gamma
High-Gamma
Information [bits]
0
0.1
0.2
0.3
SG
G
IG
Cortical Layer
ns
B
Before
During
After
alpha
nMod
gamma
h-gamma
Cortical Layer
Frequency [Hz]
20
60
100
140
Information [bits]

Figure5

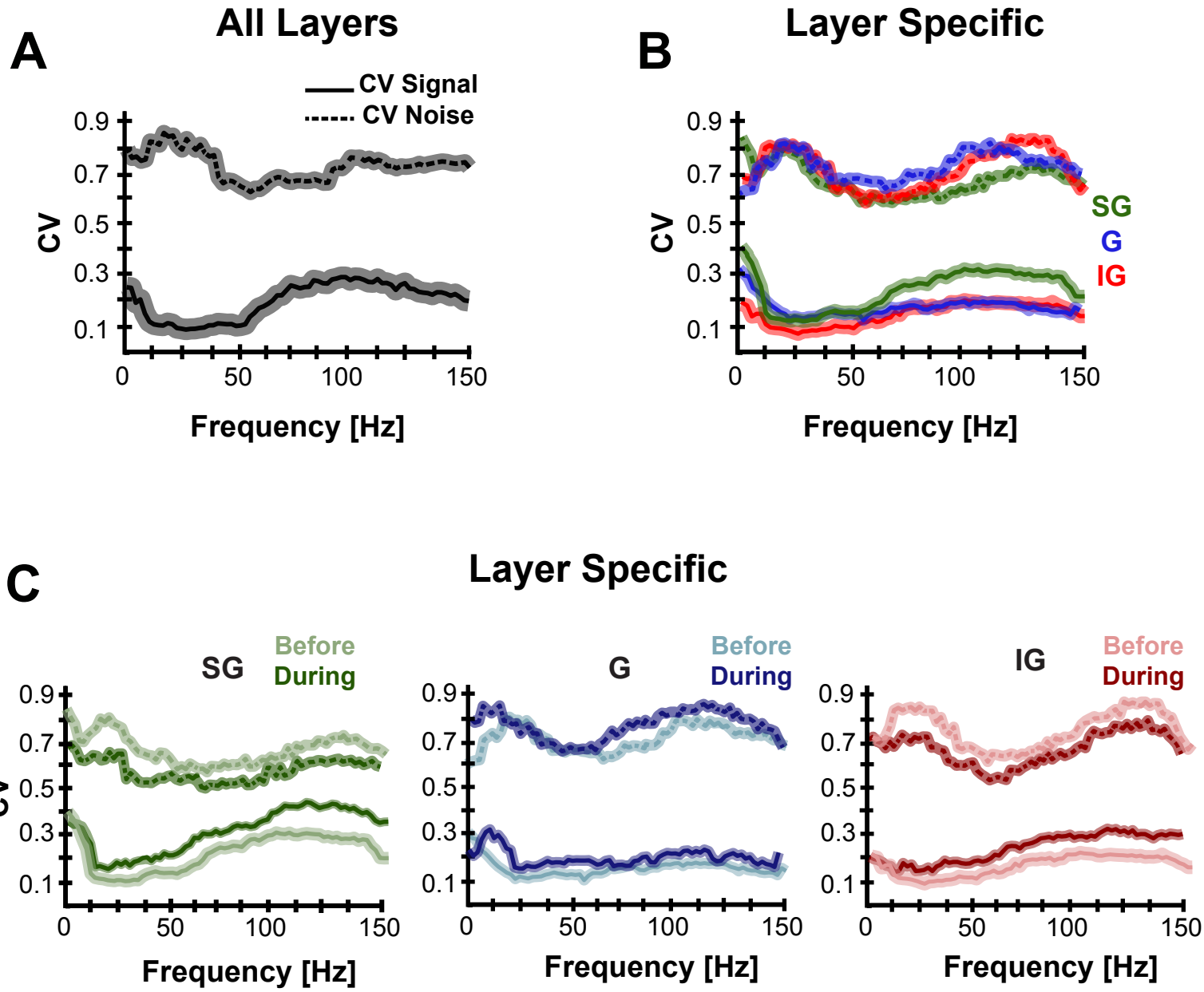
A
All Layers
CV Signal
CV Noise
CV
0.9
0.7
0.5
0.3
0.1
0
50
100
150
Frequency [Hz]
B
Layer Specific
SG
G
IG
C
Layer Specific
SG
Before
During
G
IG

Figure6

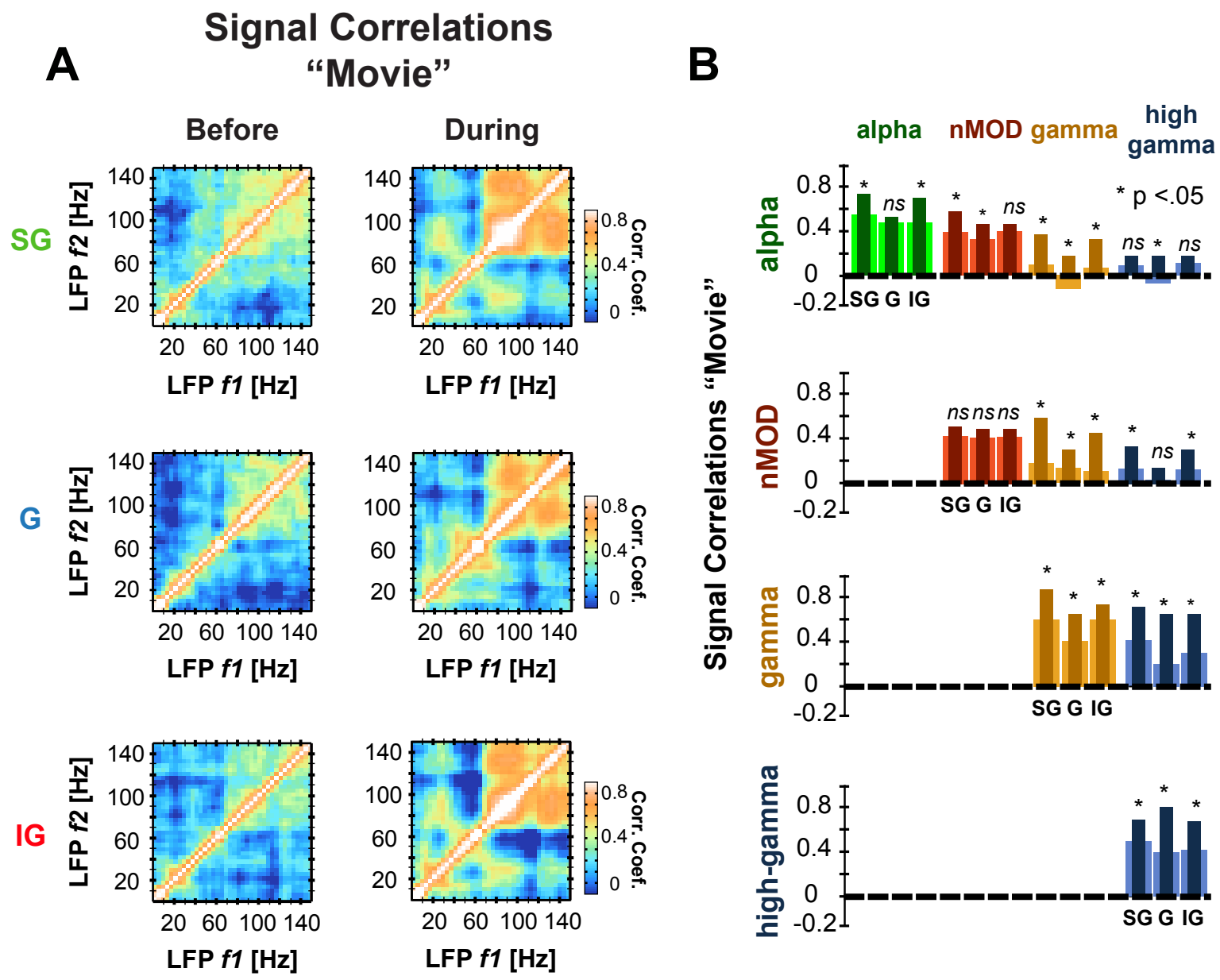
A
Signal Correlations
"Movie"
Before
During
SG
G
IG
LFP f2 [Hz]
LFP f1 [Hz]
140
100
60
20
Corr. Coef.
0.8
0.4
0
B
Signal Correlations "Movie"
alpha
nMOD
gamma
high gamma
* p <.05
ns
SG G IG
0.8
0.4
0
-0.2

SUPPLEMENTAL INFORMATION

Dopamine is signaled by mid-frequency oscillations and boosts output-layers visual information in visual cortex

Daniel Zaldivar, Jozien Goense, Scott C. Lowe, Nikos K. Logothetis, Stefano Panzeri

Supplemental Figures:

SUPPLEMENTAL FIGURE LEGENDS

Figure S1. Individual LFP-power and Information Spectrum; related to Figure 1 and Figure 2.

Average LFP power spectrum shape across all monkeys before the pharmacological injections (K07 shown in blue, n = 4; G11 shown in green, n = 3; G09 shown in red, n = 4; H09 shown in yellow, n = 4): **(A)** over the entire movie clips; **(B)** during spontaneous activity. The power spectra for each monkey were in excellent agreement with the grand average across subjects (as in Figure 2). **(C)** Information spectrum across all monkeys before pharmacology, also agrees with the results shown Figure 2. Panels **(D-F)** presents a scatterplot of power vs information, either before or during L-DOPA injection. From each experimental session and frequency, we plotted the power of the movie-evoked LFP oscillation against the information carried by the oscillation power at that frequency before **(D)** and during **(E)** the injections. These panels show that the oscillation power information is higher for higher power (as signal processing consideration would suggest) only within the boundaries of a specific stimulus-specific band. This is particularly visible for the gamma band. However, the degree of stimulus modulation changes greatly across bands. As a result, the correlation between power and information was overall weak and insignificant (before injection: rho = 0.023, p = 0.82; during injection: rho = 0.018, p = 0.71). Panel **(F)** shows the difference of movie-evoked power during and after the injection versus difference of information between during and after the injection, showing no correlation between these values (across all frequency correlation: rho = 0.012; p = 0.55). These results, besides showing that correlations between information and power were weak, also argue against a possible bias in our results toward detecting more information and DA modulation in bands with higher power (and thus higher signal-to-noise ratio). In fact, the gamma power had the second smallest power (of the bands considered), the largest visual information, and a large modulation with dopamine. Furthermore, the nMOD band had a much stronger and more discernible modulation with the L-DOPA than the alpha band, even though the alpha band had much more power.

Figure S2. CSD and Coherence Profiles from Different Monkeys Used for the Electrode Depth Alignment; related to Figure 2 and Figure 3.

(A) Average stimulus onset-triggered CSD response, for four monkeys. CSD profiles were computed before any pharmacological manipulation and for each monkey individually (K07 shown in blue, n = 4; G11 shown in green, n = 3; G09 shown in red, n = 4; H09 shown in yellow, n = 4). **(B)** Mean LFP coherence (50–100 Hz) computed between all pairs of laminar positions. This shows the inter-compartmental coherence over all sessions collected in each monkey. Note that electrode contacts in the G and SG layers show strong coherence with other G and most of the SG positions, but the coherence against IG contacts is much lower, with a sharp discontinuity. The coherence analysis helped us determine the boundaries between IG and G.

Figure S3. Example LFP traces during presentation of a 20 s long movie; related to Figure 2 and Figure 4.

Temporal courses of different LFP bands in response to the presentation of movie clips (20 s). Each plot shows neural activity from the same three trials across the selected LFP bands.

Figure S4. Noise Correlations Between Pairs of LFP Frequencies; related to Figure 6

(A) Noise correlations between pairs of LFP frequencies, before and during pharmacological injections, from different cortical depths; SG, G and IG layers (15 sessions in total). The figure shows the average noise correlation between the LFP power at frequencies, $f1$ and $f2$. No layer dependency in the

correlation was observed. The correlations between all pairs of frequencies within the nMOD-range (mean over all pairs of frequencies at 18 and 38 Hz and across all layers: 0.38±0.02) were higher than the correlation between pairs of frequencies in the α-range (mean correlations over all pairs of frequencies at 8 and 12 Hz and accords all layers: 0.24±0.03). This is fully compatible with the observations from Belitski, et al. [1] where it was reported that the nMOD range had high noise-correlations and low signal-correlations (as we observed in Figure 6). **(B)** Average correlation within and between individual LFP bands before (shown in light) and during (shown in dark) pharmacological injection. We find that the alpha range exhibited high noise and signal correlations (as seen in Figure 6), suggesting the frequencies throughout this range share sources of both signal and noise. In addition, the noise correlation between pairs of frequencies throughout the γ-range was similar in all layers (mean pairwise correlations in the gamma range: 0.13±0.03, Figure S4). No change to the noise correlation structure was observed due to the injections of L-DOPA (Figure S4B).

Figure S5. Correlations in Spontaneous Activity between pairs of LFP frequencies; related to Figure 6

(A) Spontaneously occurring correlations between pairs of different LFP frequencies, before and during pharmacological injections, from different cortical depths; SG, G and IG layers (15 sessions in total). We show the Pearson correlation between the powers observed at two different LFP frequencies, $f1$ and $f2$, during spontaneous activity, averaged over experiments. We found the correlations were highest for low frequencies (<40 Hz). We found that pairwise correlations within the nMOD range was high (mean pairwise correlations over all frequencies at 18 and 38 Hz and across all layers: 0.22±0.02) as well as the correlations between pairs of α-range (mean pairwise correlations over all frequencies at 8 and 12 Hz and across all layers: 0.23±0.02). However, the correlations between pairs of frequencies in the γ-range were the lowest (mean pairwise correlations in the gamma range: 0.08±0.03). **(B)** Average correlation within and between individual LFP bands before (light) and during (dark) pharmacological injection. We did not observe any change in the correlations structure during spontaneous activity caused by the injections of L-DOPA.

SUPPLEMENTAL FIGURES

FIGURE S1

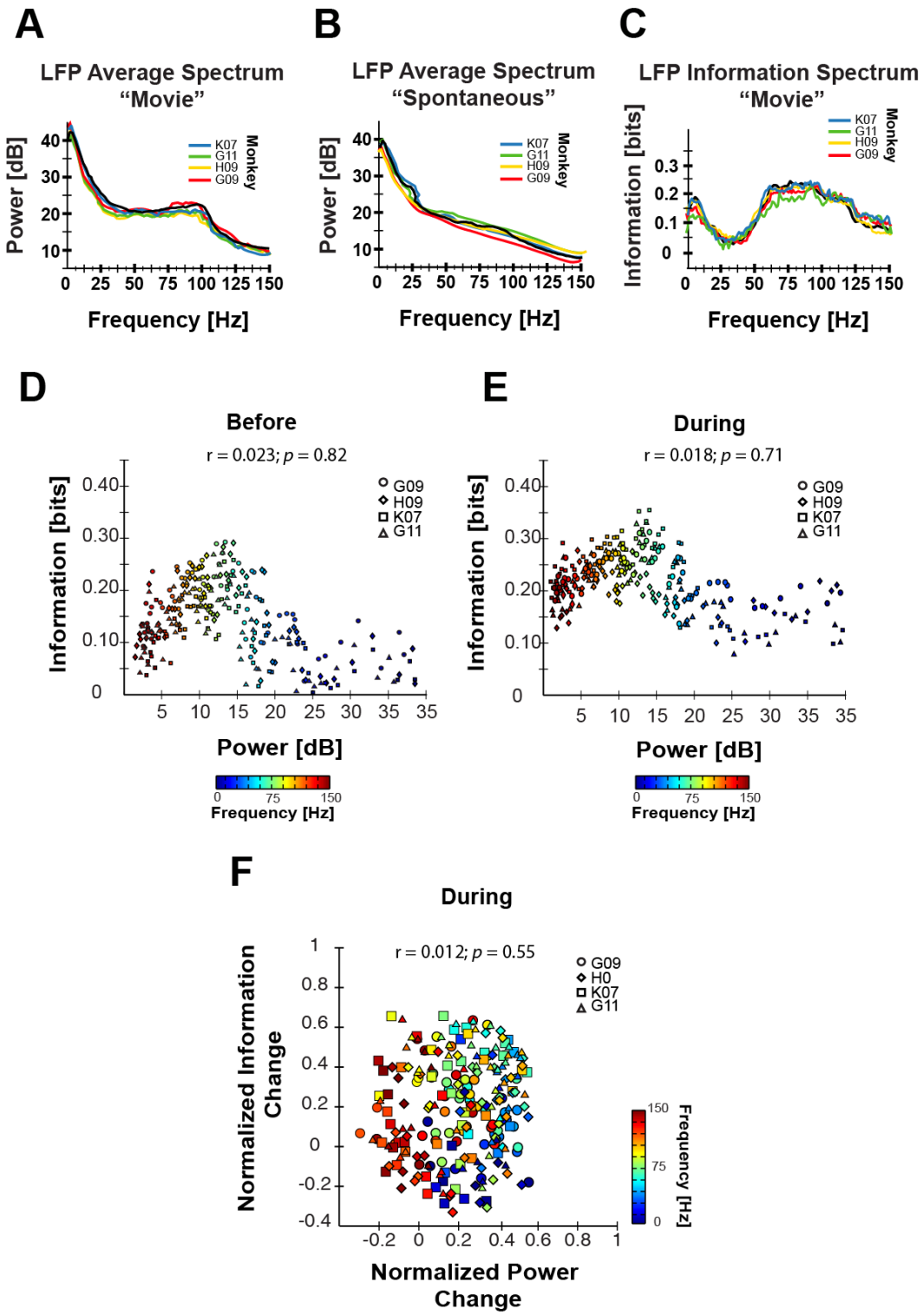

FIGURE S2

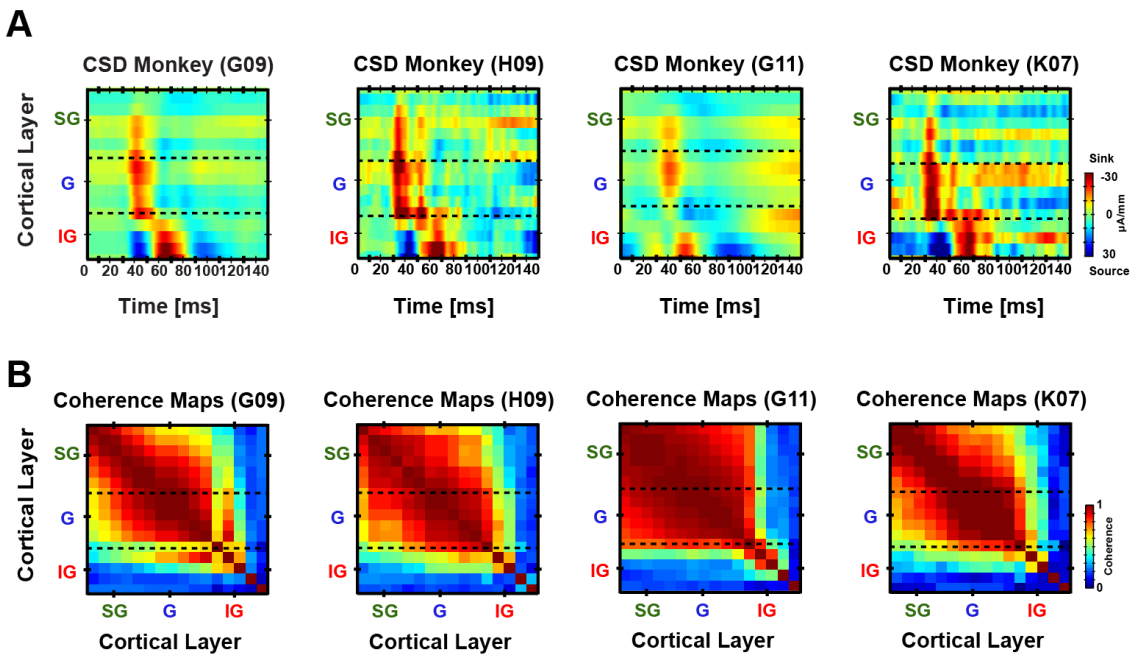
A
CSD Monkey (G09)
CSD Monkey (H09)
CSD Monkey (G11)
CSD Monkey (K07)
Cortical Layer
SG
G
IG
0 20 40 60 80 100 120 140
Time [ms]
Sink
-30
0
µA/mm
30
Source
B
Coherence Maps (G09)
Coherence Maps (H09)
Coherence Maps (G11)
Coherence Maps (K07)
Cortical Layer
Coherence
1
0

FIGURE S3

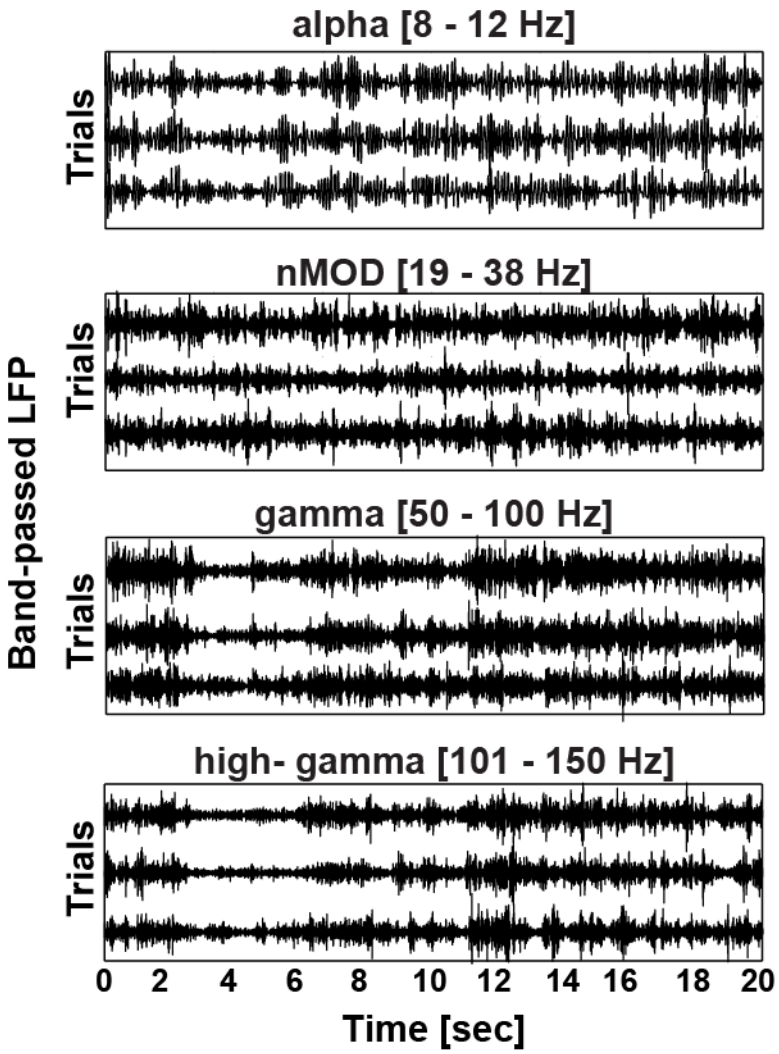
alpha [8 - 12 Hz]
nMOD [19 - 38 Hz]
gamma [50 - 100 Hz]
high- gamma [101 - 150 Hz]
Band-passed LFP
Trials
Trials
Trials
Trials
0 2 4 6 8 10 12 14 16 18 20
Time [sec]

FIGURE S4

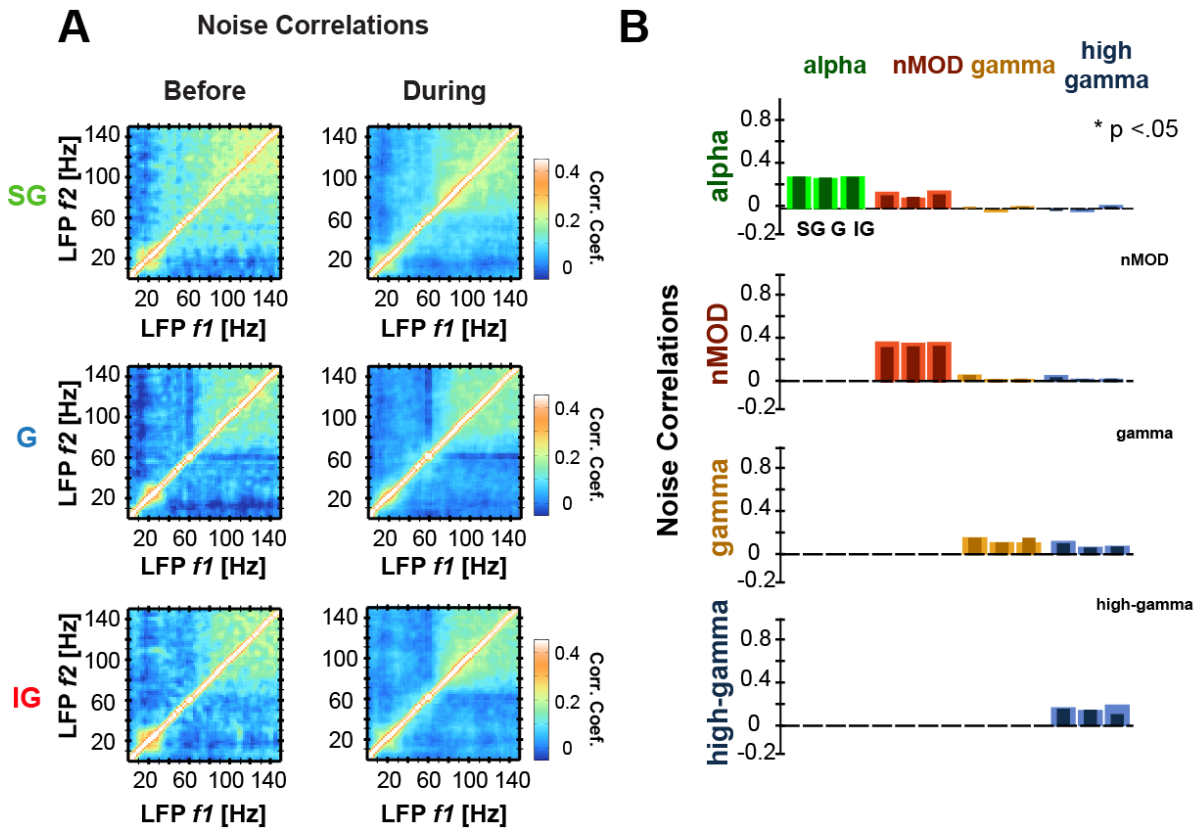
A
Noise Correlations
Before
During
SG
G
IG
LFP f2 [Hz]
LFP f1 [Hz]
20 60 100 140
Corr. Coef.
0.4
0.2
0
B
alpha
nMOD gamma
high gamma
* p <.05
Noise Correlations
SG G IG
nMOD
gamma
high-gamma
0.8
0.4
0
-0.2

FIGURE S5

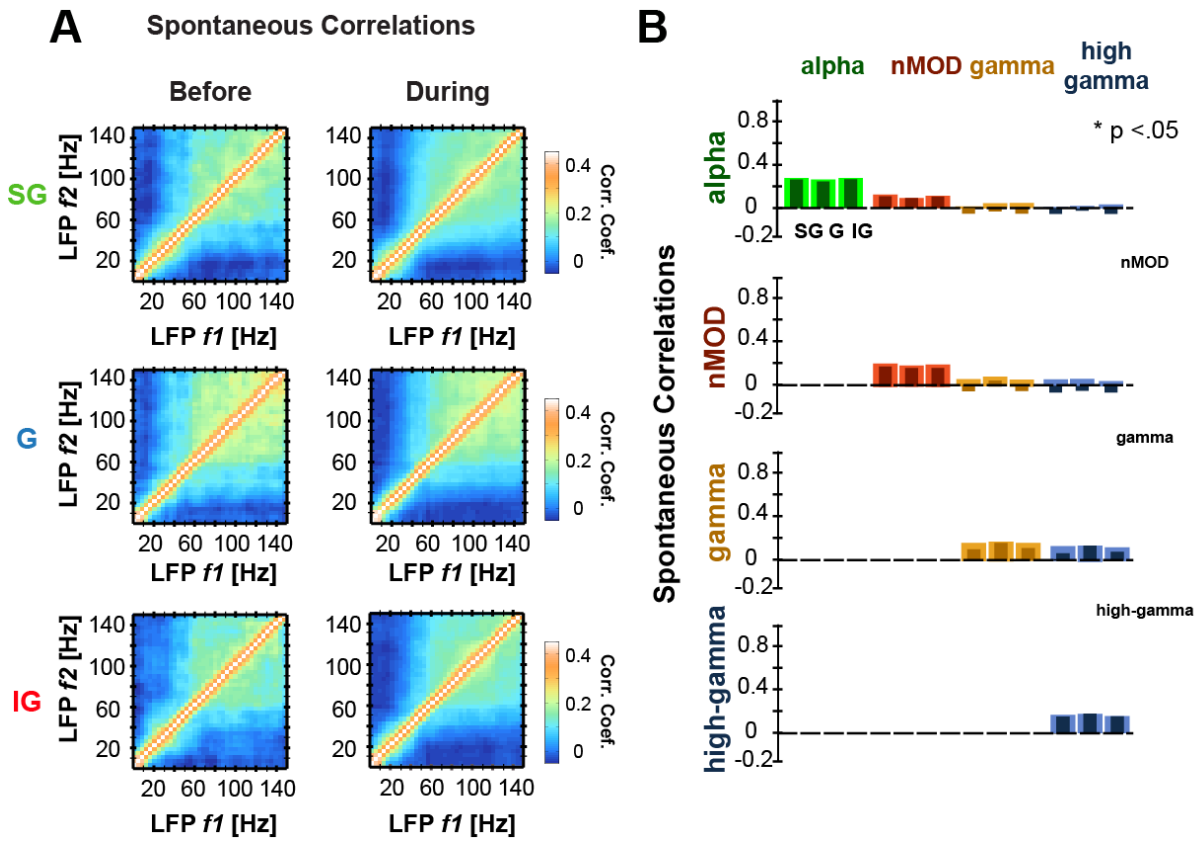
A
Spontaneous Correlations
Before
During
SG
G
IG
LFP f2 [Hz]
LFP f1 [Hz]
Corr. Coef.
B
alpha
nMOD
gamma
high gamma
* p <.05
Spontaneous Correlations
SG G IG
high-gamma